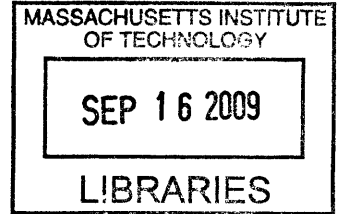


**The Design of Scaled Robotic End Effectors to
Mimic Razor Clam Burrowing**

by

Mario Attilio Bollini



Submitted to the Department of Mechanical Engineering
in partial fulfillment of the requirements for the degree of

ARCHIVES

Bachelor of Science in Mechanical Engineering

at the

MASSACHUSETTS INSTITUTE OF TECHNOLOGY

June 2009

© Mario Attilio Bollini, MMIX. All rights reserved.

The author hereby grants to MIT permission to reproduce and
distribute publicly paper and electronic copies of this thesis document
in whole or in part.

Author

Department of Mechanical Engineering
May 8, 2009

Certified by

Anette Hosoi
Associate Professor of Mechanical Engineering
Thesis Supervisor

Accepted by

John H. Lienhard V
Collins Professor of Mechanical Engineering
Chairman, Undergraduate Thesis Committee

The Design of Scaled Robotic End Effectors to Mimic Razor Clam Burrowing

by

Mario Attilio Bollini

Submitted to the Department of Mechanical Engineering
on May 8, 2009, in partial fulfillment of the
requirements for the degree of
Bachelor of Science in Mechanical Engineering

Abstract

This thesis reviews the design of two scaled mechanical end effectors that mimic the digging of *Ensis directus*, the Atlantic Razor Clam. Modeled after a 0.5x *Ensis* scale device, the end effectors are 1.0x and 2.0x *Ensis* scale. The end effectors will be coupled to a pneumatic robotic actuator to explore the nondimensional relationships governing the digging dynamics of razor clams in littoral substrates. Such dynamics could be exploited to construct novel mimetic engineering devices which would provide an order-of-magnitude improvement over existing subsea burrowing and anchoring technologies.

Thesis Supervisor: Anette Hosoi

Title: Associate Professor of Mechanical Engineering

Acknowledgments

This work was sponsored by the Batelle Memorial Institute of Columbus, OH, Bluefin Robotics of Cambridge, MA, and Chevron of Houston, TX.

I would like to thank my friends and family for the support and encouragement that made these past four years possible. Specifically, I would like to thank Thomas Vanhouten whose class inspired me to come here as student and Amos Winter whose mentoring transformed me from a student into an engineer.

Contents

1	Introduction	13
1.1	Razor Clams for Biomimetic Burrowing	13
1.2	Razor Clam Digging Dynamics	14
1.3	RoboClam Digging Apparatus	14
1.4	Current Razor Clam End Effector	15
2	Design Conceptualization	17
2.1	Important Constraints	17
2.2	Functional Requirements	17
2.2.1	Coupling Requirements	18
2.3	Kinematic Design Parameters	18
2.3.1	Wedge Design Discussion	18
2.3.2	Top Nut Design Discussion	24
2.3.3	Final Design Conceptualization	25
3	Design Analysis	27
3.1	Loading Analysis	27
3.1.1	Kinematic Constraints	27
3.1.2	Static Equilibrium Equations	27
4	Design Implementation	31
4.1	Material Selection	31
4.2	Friction Reduction	31

4.3	Mechanism Efficiency Prediction	32
4.3.1	Efficiency of Force Transfer	32
4.3.2	Efficiency of Mechanism	33
4.4	Finite Element Analysis	33
4.4.1	Shell Quarter Analysis	34
4.4.2	Wedge Analysis	34
4.5	Weight Reduction Strategies	34
4.5.1	Shell Quarters	34
4.5.2	Wedge Slider	38
4.6	Manufacturability	38
4.7	Sealing	39
5	Conclusion	41
A	1.0x End Effector Drawings	43
B	2.0x End Effector Drawings	57

List of Figures

2-1	Force balances of wedge and top-nut with rollers.	20
2-2	Requirement of wedge position underneath center of shell length. . . .	23
2-3	The 1.0x end effector assembly with components labeled.	26
3-1	The shell and wedge are exactly constrained.	28
3-2	Free body diagram of shell and wedge.	29
4-1	Stress distribution on the 2.0x scale shell quarter under loading conditions representative of the end effector opening and closing generated using finite element analysis techniques.	35
4-2	Stress distribution on the 2.0x scale wedge under loading conditions representative of the end effector opening and closing generated using finite element analysis techniques.	36
4-3	The encircled regions were lightened to reduce part weight. In the case of the 2.0x end effector shell quarter pictured, stiffening ribs were used to maintain part integrity while maximizing possible weight reduction.	37
4-4	The indicated regions were removed to reduce the part weight. The regions of remaining material were sized to minimize deflection of the wedge races during the end effector open-close cycle.	38
4-5	All of the interior features of the shell quarter can be machined from a single direction, reducing manufacturing time and cost.	39
A-1	The 1.0x scale end effector assembly	44
A-2	The 1.0x scale left shell half (drawing 1)	45

A-3	The 1.0x scale left shell half (drawing 2)	46
A-4	The 1.0x scale left shell half (drawing 3)	47
A-5	The 1.0x scale left shell half (drawing 4)	48
A-6	The 1.0x scale right shell half (drawing 1)	49
A-7	The 1.0x scale right shell half (drawing 2)	50
A-8	The 1.0x scale right shell half (drawing 3)	51
A-9	The 1.0x scale right shell half (drawing 4)	52
A-10	The 1.0x scale wedge	53
A-11	The 1.0x scale top-nut	54
A-12	The 1.0x scale end tip	55
B-1	The 2.0x scale end effector assembly	58
B-2	The 2.0x scale left shell half (drawing 1)	59
B-3	The 2.0x scale left shell half (drawing 2)	60
B-4	The 2.0x scale left shell half (drawing 3)	61
B-5	The 2.0x scale left shell half (drawing 4)	62
B-6	The 2.0x scale left shell half (drawing 5)	63
B-7	The 2.0x scale left shell half (drawing 6)	64
B-8	The 2.0x scale right shell half (drawing 1)	65
B-9	The 2.0x scale right shell half (drawing 2)	66
B-10	The 2.0x scale right shell half (drawing 3)	67
B-11	The 2.0x scale right shell half (drawing 4)	68
B-12	The 2.0x scale right shell half (drawing 5)	69
B-13	The 2.0x scale right shell half (drawing 6)	70
B-14	The 2.0x scale wedge	71
B-15	The 2.0x scale top-nut	72
B-16	The 2.0x scale end tip	73

List of Tables

4.1	The material properties of SAE 660 bearing bronze and 440C stainless steel.	32
4.2	The race angles θ , transmission ratios TR , and efficiencies η of the various scaled razor clam end effectors.	33

Chapter 1

Introduction

Biomimetic burrowing is being pursued by researchers at MIT in order to generate efficient digging and anchoring devices for use in littoral zones. Fauna from these zones were selected for study based on their ability to dig in the fluidized substrates and the hypothesis that nature has optimized these animals for underwater digging. *Ensis directus*, the Atlantic Razor Clam, was chosen because of its notable digging ability and its mechanical suitability for engineering applications [1].

The dynamics of razor clam digging are being studied with the intent of developing a set of relationships governing the digging mechanics of the animal in the fluid-soil substrate. These relationships will then be exploited to create a lightweight, low-power, reversible, subsea burrowing device. Such a device would provide an order-of-magnitude improvement over existing subsea digging and anchoring technologies [1].

This thesis discusses the design of two robotic end effectors that mimic *Ensis* burrowing behavior. Complimenting an existing end effector that is 0.5x the scale of *Ensis*, the two designed end effectors are 1.0x and 2.0x *Ensis* scale. As razor clams are approximately 6.5in in length and 1.25in in diameter [1], the 1.0x and 2.0x end effectors measure 6.5in x 1.2in x 1.2in and 13in x 2.4in x 2.4in respectively.

1.1 Razor Clams for Biomimetic Burrowing

Ensis directus, was selected for biomimetic burrowing for a number of important

reasons. Primarily, it exhibits speedy (nearly 1 centimeter per second) and energy-efficient burrowing behavior in littoral environments [2]. Additionally, *Ensis* is local to New England and instinctively digs when threatened [3], making it easy to locate in its natural environment and easy to observe while digging. *Ensis* also has merits with regards to mechanical mimicry: it has a rigid shell that performs single degree-of-freedom movement and its dimensions are of manufacturable size scales for engineering devices [1, 4].

1.2 Razor Clam Digging Dynamics

Razor clams employ a four stage digging motion [1, 3, 5]:

1. The clam foot extends to uplift the shell
2. The shell halves rapidly contract, forcing blood into the foot, inflating it to act as an anchor
3. The foot muscles contract to pull the clam downwards.
4. The shell expands

Observing *Ensis* digging in transparent substrates, Amos Winter, a PhD candidate in the Department of Mechanical Engineering at MIT who is developing the razor clam project, used particle image velocimetry to determine that the contracting movement of the shell rapidly draws water towards the clam body, unpacking and fluidizing the surrounding substrate, dramatically reducing drag on the clam [1].

1.3 RoboClam Digging Apparatus

Winter constructed an apparatus to actuate razor clam end effectors [1]. The device is powered by a SCUBA and consists of two pneumatic pistons that control the open-close and up-down motions of the end effector. The in-out motion of the end effector is actuated by a rod housed within the rod used for the up-down motion actuation.

This mechanism is compact and the components are sized to work across a range of end-effector actuation lengths.

1.4 Current Razor Clam End Effector

Winter designed and tested a 0.5x scale razor clam end effector. This prototype demonstrated that the digging dynamics of *Ensis* can be successfully mimicked by a mechanical device. It was found that the digging energy expended was similar to that expended by the razor clam.

The 0.5x scale end effector only mimics the shell movement of the razor clam. Unlike the razor clam, however, the shell halves move apart in parallel, instead of rotating apart at a hinge. This was done for mechanical simplicity and to maximize the effect of the shell movement during the open-close cycle. The end effector makes no effort to mimic the foot, as its contribution to the digging cycle is replaced by the downward force applied by the RoboClam apparatus. The similarities between the energy expended digging by the end effector and that expended digging by *Ensis* indicates that these mechanical deviations from nature do not negatively affect the performance of the device.

The design of the 0.5x scale end effector was driven primarily by the size constraints of the device. A sliding wedge was used to open and close the device because of its simplicity and the requirements dictating that the 0.5x end effector open as wide as an actual razor clam (0.25in). While in operation several observations were made of the end effector's performance that were used to improve the design of the 1.0x scale and 2.0x scale devices.

The primary observation was that the quick impulse of the closing motion was deforming the inner rod causing it to rub against the top nut and introducing unexpected and uncharacterizable friction. The slider was designed to open the clam while being pulled by the inner rod, to reduce the chances of the rod buckling under the expected high load on the clam while it was opening.

Chapter 2

Design Conceptualization

The design of the end effectors was accomplished by studying the 0.5x scale end effector, reviewing the functional requirements that the components needed to satisfy, and narrowing down potential implementations on the basis of technical feasibility and ease of design and manufacture.

2.1 Important Constraints

The key constraints that limited the scope of end effector designs were:

1. The end effectors cannot require special mechanical modifications to attach to the existing RoboClam device.
2. The end effectors cannot be made out of materials prone to corrosion.
3. The end effectors cannot be exposed to particles at risk of jamming.

2.2 Functional Requirements

Building off of the constraints, the functional requirements for the 1.0x and 2.0x scale end effectors were:

1. The end effectors must attach to the existing RoboClam mechanism.

2. The end effectors must be 1.0x and 2.0x the scale of razor clams.
3. The end effectors must open approximately half of their thickness (0.5in for the 1.0x scale and 1.0in for the 2.0x scale end effectors).
4. The materials used must be saltwater tolerant.
5. The mechanisms must be sealed from sand particles.
6. The end effectors must perform repeatably during high frequency testing cycles.
7. The end effectors must be sealed or otherwise tolerant of substrate particulates.
8. The efficiency of the mechanisms must be characterized theoretically for use in energy calculations.

2.2.1 Coupling Requirements

Both the 1.0x and 2.0x scale end effectors were required to couple to the RoboClam actuator using the existing coupling mechanism. This requires that the open-close motion be controlled by the in-out movement of the inner rod and that the up-down motion of the devices be controlled by the up-down movement of the outer rod.

2.3 Kinematic Design Parameters

A variety of internal mechanisms were considered to satisfy the set of functional requirements. The final mechanism was selected based on its ease of design and manufacture, simplicity, and scalability to work for both the 1x and 2x scale end effectors.

2.3.1 Wedge Design Discussion

While a number of linkage mechanisms were considered for the end-effector actuation, it was quickly determined that a wedge-based approach similar to the 0.5x scale end effector would be the simplest and most effective option. The primary design

deliberations then fell on deciding whether to utilize a sliding wedge or a wedge that had rolling bearing contacts.

Axle Bending Calculations

A first order loading analysis was performed on the bearing axles to estimate the minimum axle diameter required to avoid failure. The loading configuration was modeled after the 0.5x end effector.

Figure 2.3.1(a) shows a free body diagram of the wedge with rollers. At static equilibrium, the normal forces on the two ends of four axles, F_N , balance the pulling force F_{piston} of the inner rod:

$$F_{piston} = 2 \times 4 \times F_N \sin(\theta), \quad (2.1)$$

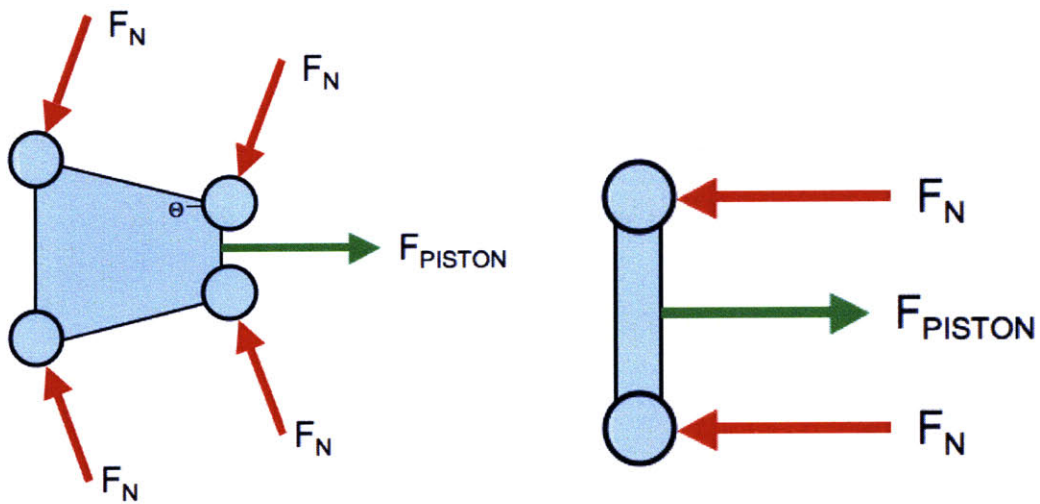
where θ is the angle of the races from the side of the clam. Thus,

$$F_N = \frac{F_{piston}}{8 \sin(\theta)}. \quad (2.2)$$

Given that the pistons are operated at 100 psi and the surface area of the pistons are 1 and 1.25 squared inches (for the close and open motions respectively), the maximum force F_{piston} is 125 pounds force, or 556 Newtons. Estimating an angle θ of 7° scaled from the 0.5x scale end effector,

$$F_N = \frac{556N}{8 \times \sin(7^\circ)} = 1140N \quad (2.3)$$

The axles would be cantilevered a distance of approximately 0.25 inches and would have evenly distributed loading across the cantilevered lengths which would be in contact with the races on the shell quarters. Assuming even loading across the length of the axles, we can simplify the distributed loading as a point load at 0.125 inches or 3.175×10^{-3} meters cantilevered length.



(a) The force balance on the wedge with rollers. (b) The force balance on the top-nut with rollers.

Figure 2-1: Force balances on the wedge and top-nut with rollers. Note that only half of the reaction forces on the axles are shown, as the reaction forces overlap when viewed from the side.

The maximum stress σ_{max} on a rod in pure bending is given by the relation

$$\sigma_{max} = \frac{F_N L r}{I_{rod}}, \quad (2.4)$$

where F is the applied force on the rod, L is the length at which the force is applied, r is the radius of the rod, and I_{rod} , the moment of the inertia of the rod about the bending axis is, is given by

$$I_{rod} = \frac{\pi r^4}{4}. \quad (2.5)$$

Solving for the radius r , one finds that

$$r = \left(\frac{4 F_N L}{\pi \sigma_{max}} \right)^{1/3}. \quad (2.6)$$

Using the known yield strength, σ_y for the 18-8 stainless steel axles of approximately 290 MPa [6] and a safety factor of 2, we will aim for a maximum stress, σ_{max} , of 145 MPa. Inserting these values along with the calculated axle force from Equation 2.3 into Equation 2.6, we find

$$r = \left(\frac{4 \times 1140N \times 3.175 \times 10^{-3}m}{\pi \times 145MPa} \right)^{1/3} = 0.0032m = 0.126in \quad (2.7)$$

We can now use this calculated radius value to estimate whether the end effector will be able to meet its opening distance requirements.

Geometric Opening Distance Calculations

We can find the maximum possible opening distance as a function of the shell and wedge geometry by determining the change in height of a roller axle at the beginning and at the end of a stroke.

At the beginning of the stroke, the height of the roller center above a datum at the bottom of the shell is simply the radius r , or

$$y_1 = r. \quad (2.8)$$

At the end of the stroke, the height of the roller center above the datum is a function of the radius of the roller, the horizontal length of the slider L , the height of the shell quarter H and the angle of the race and slider incline θ ,

$$y_2 = H - r - L \tan(\theta). \quad (2.9)$$

The distance d the shells can open is $2(y_2 - y_1)$, or

$$d = 2(H - 2r - L \tan(\theta)). \quad (2.10)$$

For the 1.0x scale end-effector, scaling off of the 0.5x device, we can estimate a length L of 2in , a height H of 0.6in, and an angle of 7° . Substituting into Equation 2.10, we find

$$d = 2(0.6in - 2 \times 0.126in - 3in \times \tan(7^\circ)) = 0.20in. \quad (2.11)$$

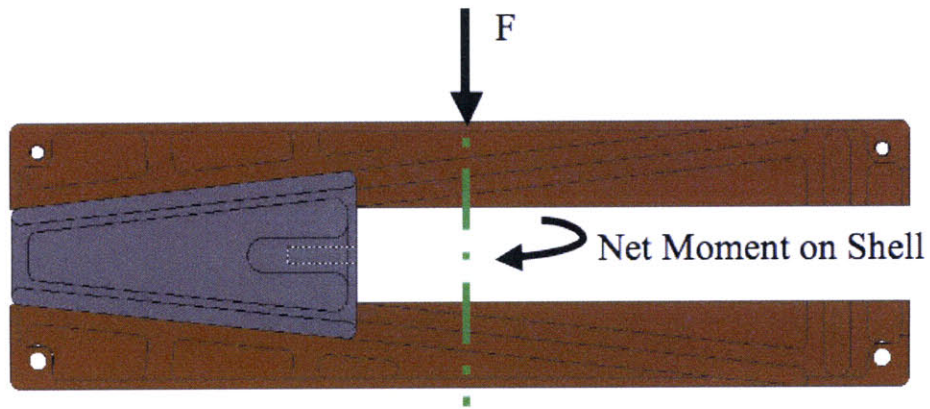
This is lower than the required 0.5in opening distance for the 1.0x end effector. The value d could be increased by decreasing the angle θ and the length L , but these changes would be infeasible because of geometric sizing constraints and the necessity to maximize the length of the wedge with respect to its width to prevent it from binding in the shell races.

Equations 2.1-2.11 demonstrate that any appropriately sized axles would cause the device to fail meet the opening distance requirements of 0.5in for the 1.0x end effector and 1.0in for the 2.0x end effector. Thus, a wedge with rolling contacts does not meet the loading and geometry requirements.

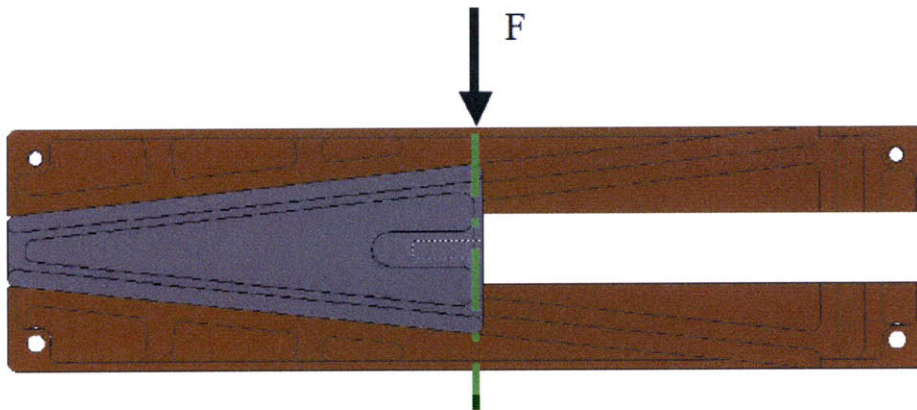
Wedge Length Determination

Several factors determined the minimum length of the wedge. The first was the necessity to have a length to width ratio of greater than two to avoid jamming in the races. The second factor was the requirement that the wedge always has to lie under the center of pressure on the shell to prevent moments on the shell. Figure

2-2 demonstrates this requirement. If the wedge is too short as in Figure 2-2(a) a net moment is produced by the average force on the shell surface. This net moment invalidates the equilibrium equations used to characterize the system. If the wedge is always underneath the center of the shell length, as is guaranteed if the wedge length is greater than half that of the shell, no net moment is produced, as is illustrated in Figure 2-2(b).



(a) When the wedge is not under the center of the shell length, a net moment is produced.



(b) When the wedge is under the center of the shell length, no net moment is produced.

Figure 2-2: The effects of the wedge position on net moments produced on the shell by the average force acting on its outer surface.

2.3.2 Top Nut Design Discussion

Rolling contacts could prove feasible for the top-nut, with the lack of geometric constraints and the order of magnitude lower loading calculated in Equation 2.12. This would provide an advantage over the 0.5x scale end effector by providing a lower friction contact.

Axle Bending Calculations

Figure 2.3.1(b) shows a free body diagram of the top nut. The four rolling contact points would balance the force F of the loading bar, thus the normal force N acting on each axle would be

$$F_N = \frac{F}{4}. \quad (2.12)$$

With $F = 556N$, we find that $F_N = 139N$. Substituting into Equation 2.6, we see that the minimum radius is 0.0026m, or 0.102inches, within the available sizes for rolling elements and well within the geometric space requirements for this component.

Rolling Contact Force Calculations

Utilizing a $\frac{3}{16}$ in (0.0047m) diameter rolling pin (for ease of potential bushing sizing), we utilize Hertzian stress equations to ensure that the rolling element does not create locally high contact stresses on the shell race surface.

For a rolling cylinder on a flat surface, the Hertzian constant equation [7] can be used to calculate the size of the surface pressure area. Equation 2.13 shows that the half width of the contact patch, b , is

$$b = \sqrt{\left(\frac{2F}{\pi L}\right) \left(\frac{\frac{1-\nu_1^2}{E_1} + \frac{1-\nu_2^2}{E_2}}{\frac{1}{d_1}}\right)}, \quad (2.13)$$

where ν_1 and ν_2 are the Poisson's ratios and E_1 and E_2 are the moduli of elasticity of the pin and surface materials respectively, d_1 is the diameter of the pin, F is the loading force pressing the pin into the surface, and L is the pin contact length.

The pressure p_{max} on the surface is given by Equation 2.14 [7]:

$$p_{max} = \frac{2F}{\pi bL}. \quad (2.14)$$

Substituting in the material properties of bronze and steel for the shell and pin respectively, estimating a pin contact length L of 0.0032 m (0.125 in), using the pin diameter of 0.0048 m ($\frac{3}{16}$ in), and with our calculated force F_N of 139 Newtons, we find

$$b = \sqrt{\left(\frac{2 \times 139N}{\pi \times 0.0032m}\right) \left(\frac{\frac{1-0.27^2}{200 \times 10^9 Pa} + \frac{1-0.34^2}{120 \times 10^9 Pa}}{\frac{1}{0.0048m}}\right)} = 4.23 \times 10^{-5}m. \quad (2.15)$$

Thus,

$$p_{max} = \frac{2 \times 139N}{\pi \times 4.23 \times 10^{-5}m \times 0.0032m} = 659MPa. \quad (2.16)$$

This value is approximately 5 times larger than the yield strength $\sigma_{max} = 125MPa$ of the bronze used in the shell, demonstrating that a four roller solution would not be feasible for the top-nut to shell contact. Doubling the contact lengths, increasing the pin diameters, and increasing the number of pins would reduce the contact pressure, but would also press the limits of the sizing requirements and add complexity to the part. As a result a sliding contact was chosen for this constraint instead.

2.3.3 Final Design Conceptualization

Sliding wedge and sliding top-nut mechanisms were selected for both the 1.0x and 2.0x scale end effectors. Figure 2-3 shows the 1.0x end effector with the key components labeled. The 2.0x end effector is kinematically identical to the 1.0x device. The primary differences between the two devices can be attributed to weight reduction and the strategic reinforcement of the scaled parts in the 2.0x scale end effector. Engineering drawings of the components for the 1.0x and 2.0x end effectors can be found in Appendix A and Appendix B respectively.

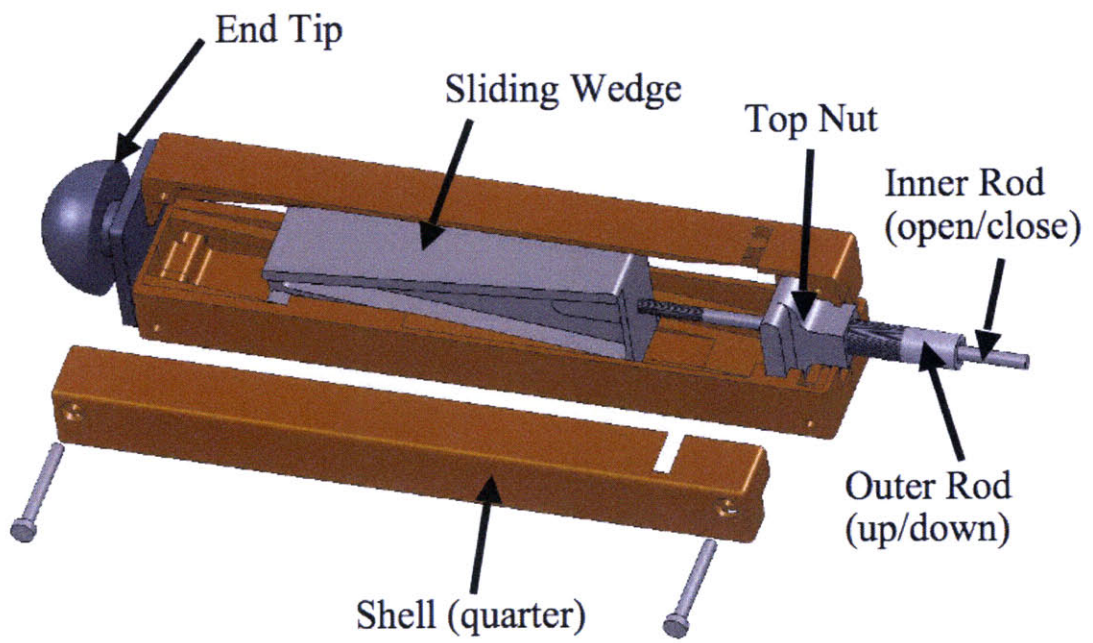


Figure 2-3: The 1.0x end effector assembly with components labeled.

Chapter 3

Design Analysis

3.1 Loading Analysis

3.1.1 Kinematic Constraints

The 1.0x and 2.0 end effectors are both exactly constrained and can be deterministically characterized. Figure 3-1 shows the mechanism constraints. Vertical motion and rotation about the lateral axis are constrained by the interface between the shell races and the wedge. Horizontal motion and rotation about the vertical axis are constrained by the interface between the interior side surface of the shell and the sides of the wedge. Axial motion is prevented by the interface between the top-nut races and the shell. Rotation about the longitudinal axis is prevented by the interface between the shell races and the wedge.

3.1.2 Static Equilibrium Equations

Shell Equilibrium

Referencing the shell and forces illustrated in Figure 3-2 and summing the axial forces at equilibrium, we find:

$$\Sigma F_x = -T + N \sin(\theta) + \mu N \cos(\theta) = 0 \quad (3.1)$$

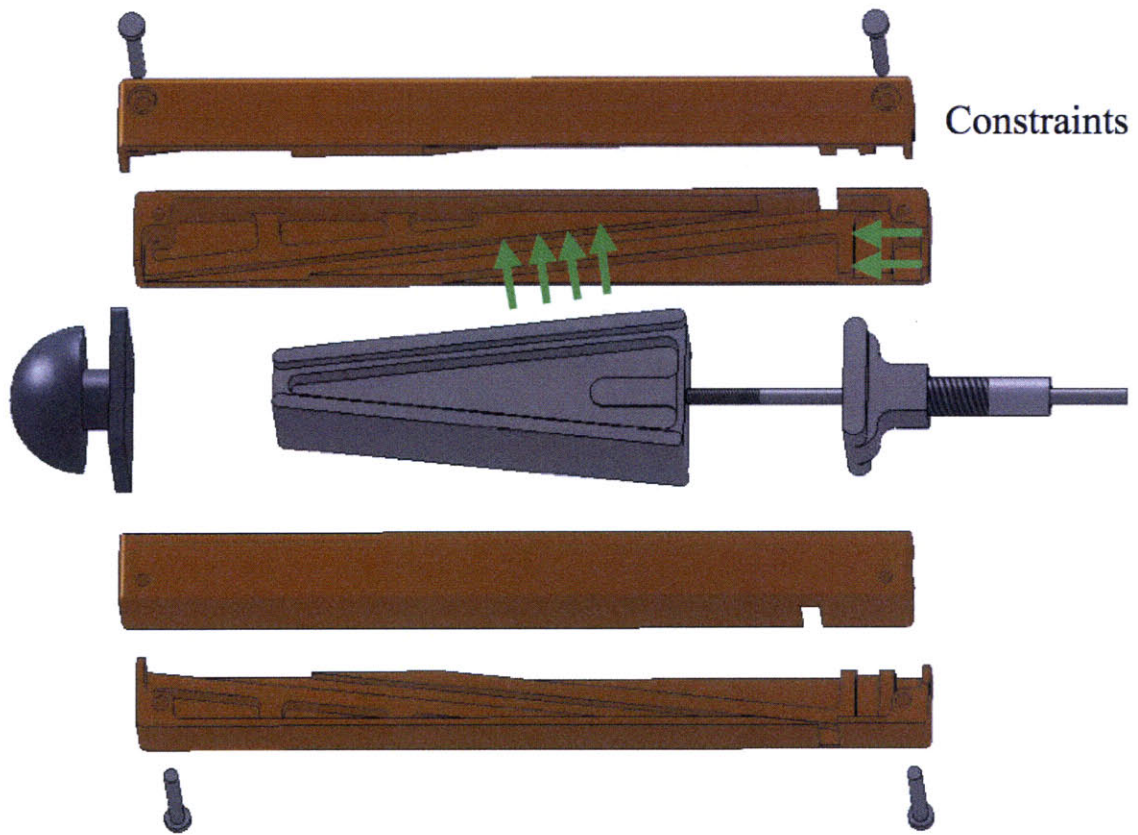


Figure 3-1: The shell and wedge are exactly constrained.

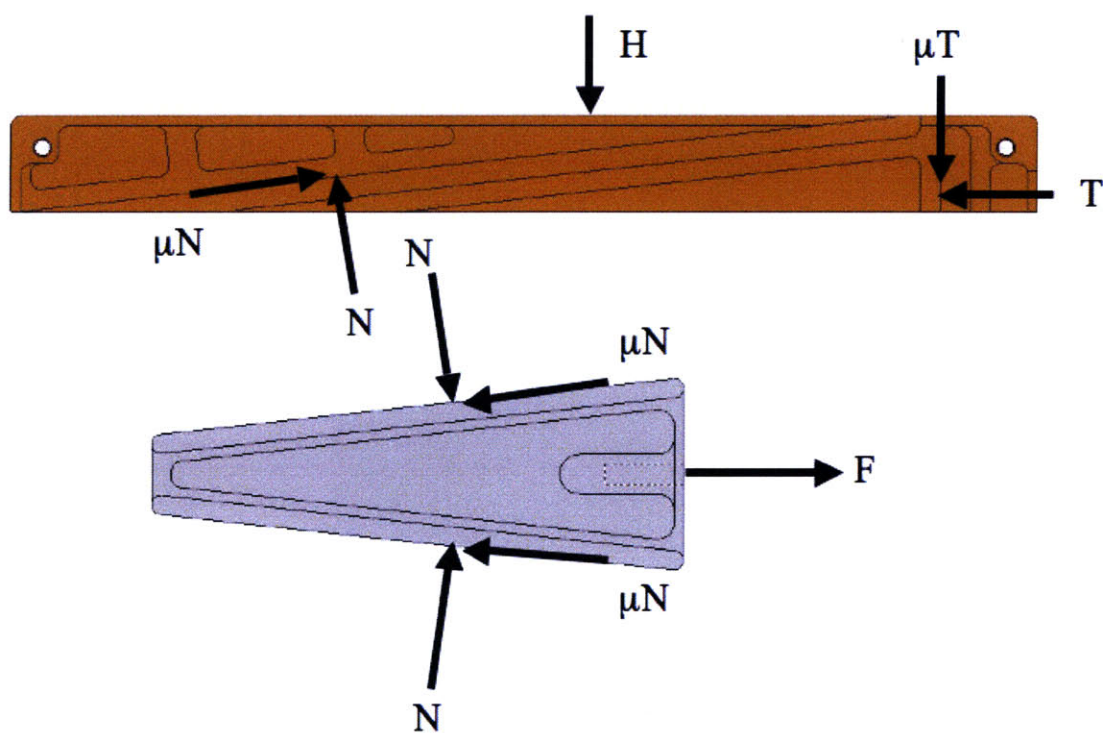


Figure 3-2: Free body diagram of shell and wedge.

Summing the lateral forces at equilibrium, we find:

$$\Sigma F_y = H - N\cos(\theta) + \mu N\sin(\theta) + \mu T = 0. \quad (3.2)$$

Wedge Equilibrium

Referencing the wedge and forces illustrated in Figure 3-2 and summing the axial forces at equilibrium, we find:

$$\Sigma F_x = F + 2N\sin(\theta) - 2\mu N\cos(\theta) = 0 \quad (3.3)$$

Symmetry provides that the lateral forces on the wedge self-cancel.

Chapter 4

Design Implementation

4.1 Material Selection

The loadings experienced by the end effector coupled with the saline operating environment significantly narrowed the scope of feasible engineering materials. Inherent to the wedge design approach is the sliding interface between the wedge slider and the shell. This placed an additional constraint, requiring that the materials selected comprise a low-friction bearing surface.

With these constraints in mind, the shell quarters were designed of SAE 660 bearing bronze, which is corrosion resistant in salt water, extremely hard, and an excellent bearing surface. The slider wedge, end cap, and top nut were designed of 440C stainless steel, which met the loading requirements, comprised a low-friction bearing surface when coupled with the bearing bronze, and had acceptable corrosion resistance [8].

4.2 Friction Reduction

There are three regions of moving contact where friction between components is of concern:

1. Between the end-tip and the shells

	SAE 660 Bearing Bronze	440C Stainless Steel
Modulus of Elasticity [<i>GPa</i>]	100	200
Yield Strength [<i>MPa</i>]	125	1230
Poisson's Ratio [1]	0.34	0.27
Density [<i>g/cm</i> ³]	8.93	7.8

Table 4.1: The material properties of SAE 660 bearing bronze [9, 10] and 440C stainless steel [11, 12]

2. Between the sliding wedge and the shells
3. Between the top-nut and the shells

All of these contact surfaces represent an interface between two components composed out of the two selected materials, brass and steel. This material interface was selected in part because of its low friction when lubricated [8]. Silicon based lubricant was used to prevent absorption by the neoprene boot surrounding the apparatus.

4.3 Mechanism Efficiency Prediction

4.3.1 Efficiency of Force Transfer

The transmission ratio, TR , is analogous to the ratio for the 0.5x scale end effector, and is given by Equation 4.1 which follows from Equations 3.1, 3.2, and 3.3.

$$TR = \frac{H}{F} = \frac{1}{2} \left(\frac{\cos(\theta) - \mu \sin(\theta)}{\sin(\theta) + \mu \cos(\theta)} - \mu \right), \quad (4.1)$$

where θ is the angle the of the shell race, and μ is the coefficient of sliding friction at the brass-steel interface.

Using $\mu = 0.173$ [1] from the 0.5x end effector and with $\theta = 6.09^\circ$ for the 1.0x device and $\theta = 5.71^\circ$ for the 2.0x device, we can estimate that $TR = 1.67$ and

	0.5x clam	1.0x clam	2.0x clam
θ	7.13°	6.09°	5.71°
TR	1.55	1.67	1.69
η	0.39	0.354	0.348

Table 4.2: The race angles θ , transmission ratios TR , and efficiencies η of the various scaled razor clam end effectors [1].

$TR = 1.69$ for the 1.0x and 2.0x devices respectively. In comparison, the transmission ratio for the 0.5x scale end effector is 1.55.

4.3.2 Efficiency of Mechanism

The efficiency of the mechanism is also analogous to the efficiency of the 0.5x scale end effector, and is given by Equation 4.2 [1]:

$$\eta = \frac{E_{in}}{E_{out}} = 2 \frac{H\delta_x}{F\delta_y} = 2TR\sin(\theta), \quad (4.2)$$

where TR is the transmission ratio calculated in Equation 4.1. Substituting values obtained from Equation 4.1, we find that the estimated efficiencies for the 1.0x and 2.0x devices are $\eta = 0.354$ and $\eta = 0.348$ respectively. In comparison, the efficiency of the 0.5x scale end effector is 0.39.

Table 4.3.2 compares the transmission ratios and efficiencies of the end effectors.

4.4 Finite Element Analysis

Finite element analysis techniques were used to validate the integrity of the end effector components under expected loading conditions. The approach was used primarily to locate regions of redundant support in order to identify part features to be minimized or removed to reduce part weight. The parts most extensively studied were the shell quarters and the wedges.

4.4.1 Shell Quarter Analysis

The shell quarters were analyzed using a loading of 1500 N normal force on each race surface over a region the same size as the sliding wedge. The normal force value was determined from the force experienced by the races when the device is in mechanical static equilibrium. A fixed restraint was placed along the shell bottom and a rolling restraint was placed along the race where the top-nut would be in contact with the shell. Figures 4-1(a) and 4-1(b) illustrate the stress distributions calculated for these loading conditions for the opening and closing motions of the end effector respectively.

4.4.2 Wedge Analysis

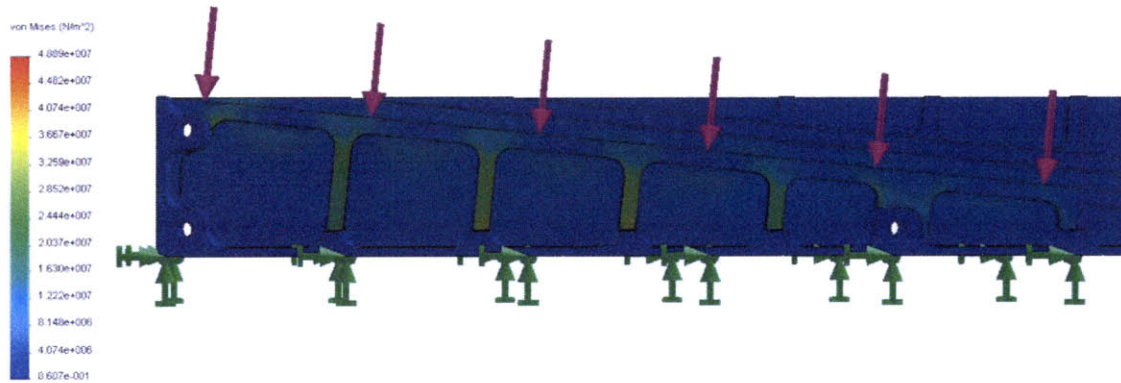
The wedges were analyzed using a loading of 1500 N normal force on each race surface. The wedge was analyzed with all four races loaded simultaneously. The restraint was placed along the inner surface of the tapped hole where the inner rod connects to the wedge. Figures 4-2(a) and 4-2(b) illustrate the stress distributions calculated for these loading conditions for the opening and closing motions of the end effector respectively.

4.5 Weight Reduction Strategies

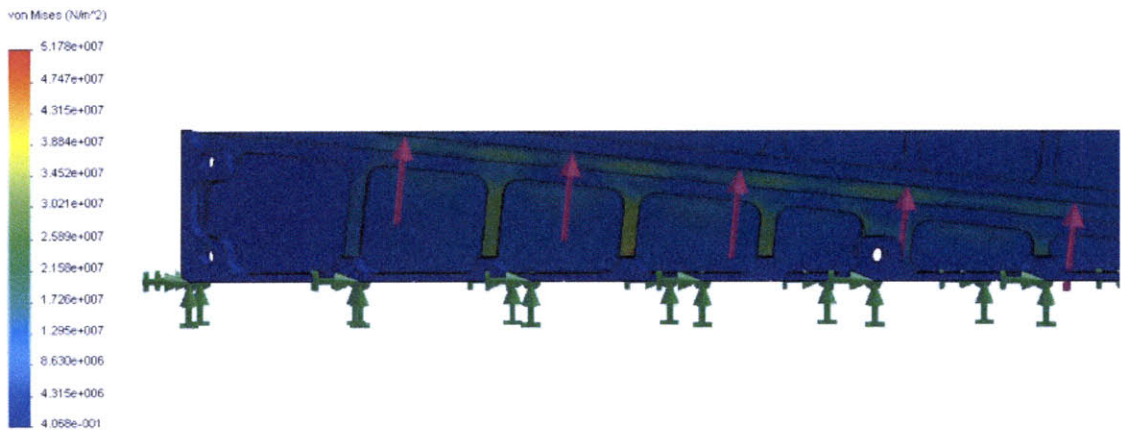
In order to minimize the inertial effects on the apparent dynamics of the clam digging, considerable care was taken to reduce the weight of the end-effectors as much as possible, particularly on the 2x scale clam. The weight reduction approach was iterative, going through repeated cycles of force path analysis, material removal, and validation with finite element analysis techniques.

4.5.1 Shell Quarters

The shell quarter undergoes two distinct phases of loading during the opening and closing phases of the clam digging cycle. Figures 4-1(a) and 4-1(b) illustrate the primary loading paths on the shell quarter during these phases. When the clam is

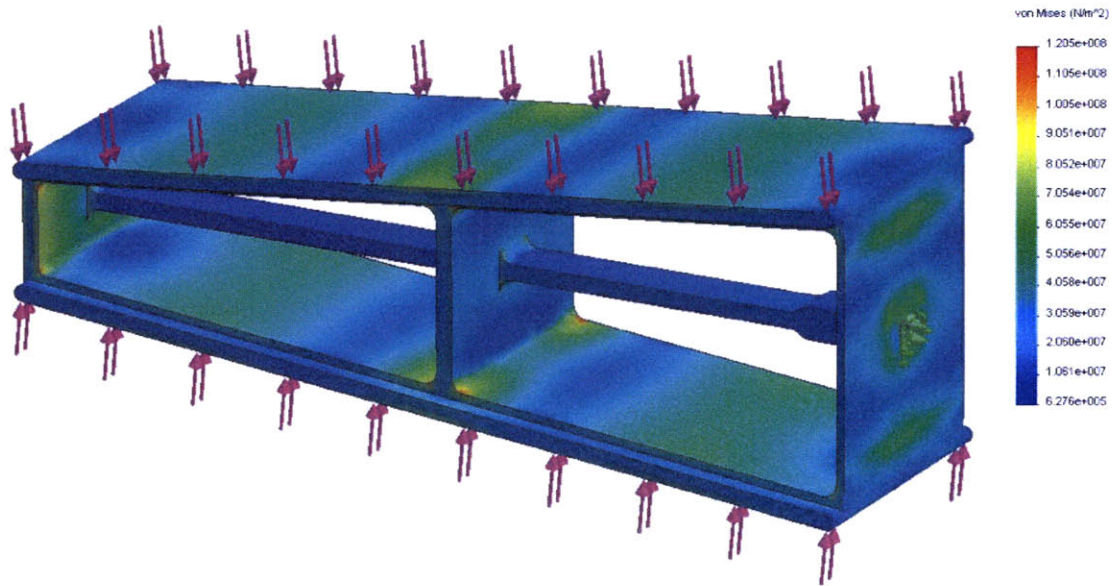


(a) Loading conditions representative of the end effector opening

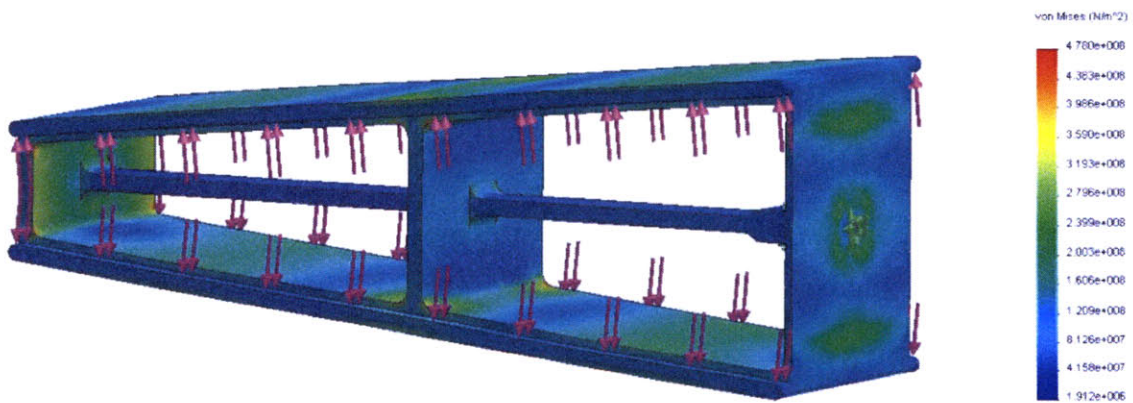


(b) Loading conditions representative of the end effector closing

Figure 4-1: Stress distribution on the 2.0x scale shell quarter under loading conditions representative of the end effector opening (a) and closing (b) generated using finite element analysis techniques. The shell material is SAE 660 Bearing Bronze, with $\sigma_y = 125MPa$.



(a) Loading conditions representative of the end effector opening.



(b) Loading conditions representative of the end effector closing.

Figure 4-2: Stress distribution on the 2.0x scale wedge under loading conditions representative of the end effector opening (a) and closing (b) generated using finite element analysis techniques. The wedge material is 660C Stainless Steel, with $\sigma_y = 1.65GPa$.

opening, the loading path is between the outer slider race and the outermost surface of the shell. To reduce weight, this region was hollowed out and reinforced with loaded ribs between the race and the surface. Additionally, the bottom surface on the 2x clam was reinforced with stiffening ribs to increase its moment of inertia to resist bending while preserving its relative thinness. Due to the 1x clam's shorter cantilevered length, ribs were not required to prevent bending of the surface.

During the clam closing phase, the loading path is between the innermost slider race and the same outer surface of the shell. The closing force applied to the race is transmitted through the side wall of the shell to the bottom. The inner offset of the race relative to the side wall results in an applied moment. This moment was resisted by thickening of the side wall between the two slider races. The aforementioned loaded ribs also served to resist the bending moment. The region of the shell between the inner race and the axis of the clam is primarily loaded by the compressive pressure of the sealing tube. This comparatively low loading allowed the region to be hollowed out on the 1x scale clam. The larger cantilevered length on the 2x scale clam, however, required this region to be reinforced with thin ribs to prevent accidental bending.

The region of the shell quarters around the top nut slider received relatively lower loads and were hollowed out where possible while maintaining the minimum 0.125 inch loaded race thickness. Figure 4-3 indicates the regions of the shell quarter where substantial amounts of material were removed to reduce part weight.

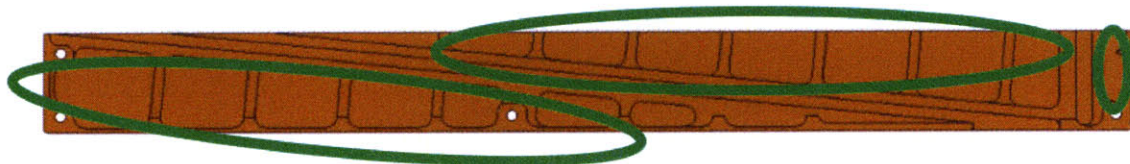


Figure 4-3: The encircled regions were lightened to reduce part weight. In the case of the 2.0x end effector shell quarter pictured, stiffening ribs were used to maintain part integrity while maximizing possible weight reduction.

4.5.2 Wedge Slider

The wedge slider, the primary kinetic component of the assembly, received particular care in weight reduction. Figures 4-2(a) and 4-2(b) illustrates the loading paths during the opening and closing phases of the digging cycle. The strategy for this component was to minimize the deflections of the sliding races while eliminating all unloaded regions of the slider. This was accomplished by thickening the region of the slider leading out to the races, increasing its moment of inertia to resist the moments exerted.

The large size of the slider on the 2x scale clam allowed its interior to be hollowed out while preserving the integrity of the loading paths. The supportive struts were sized to support the compressive loads without buckling. Figure 4-4 indicates the regions of the 2x scale end effector wedge that were removed to decrease the part weight.

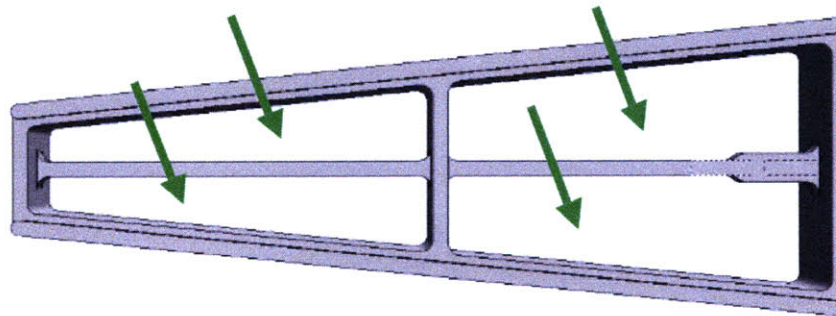


Figure 4-4: The indicated regions were removed to reduce the part weight. The regions of remaining material were sized to minimize deflection of the wedge races during the end effector open-close cycle.

4.6 Manufacturability

The hardness of the materials selected along with the feature and surface accuracies required presented challenges to the manufacture of the components of the end effector

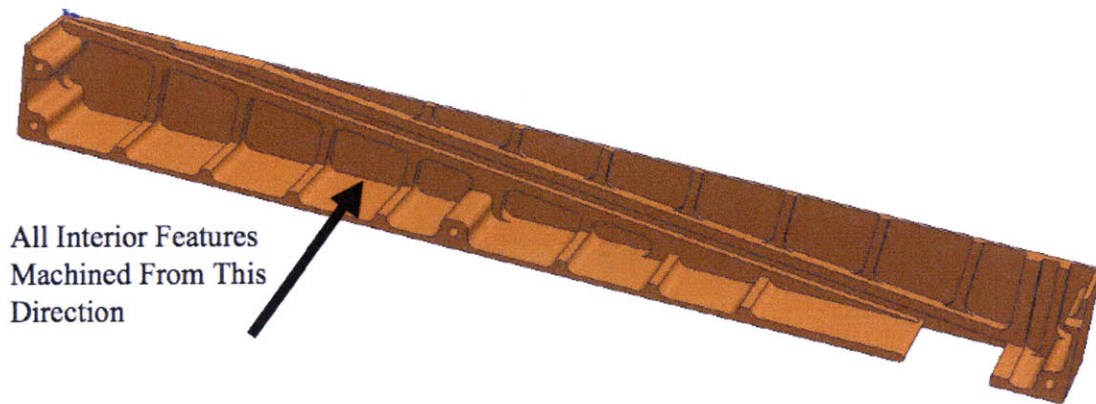


Figure 4-5: All of the interior features of the shell quarter can be machined from a single direction, reducing manufacturing time and cost.

assemblies. The complexity and size of the shell quarters required that care be taken to design the components for ease of manufacture.

As outlined in Figure 4-5, the shell quarters are designed to be machined from a single direction, reducing the need for refixturing. The minimum fillet size of the 2x shell quarter, which contains a significant amount of ribbing for weight reduction, was increased to a diameter of 0.25 inches to decrease manufacturing time and cost.

All dimensions on the components are measured from a set of three datums, reducing the effects of tolerance stacking.

4.7 Sealing

The component must be sealed to prevent the introduction of sand to the bearing surfaces while the clam is digging. This is accomplished by placing the end-effector in a neoprene boot and sealing the boot against the groove of the end-tip and a rubber stopper surrounding the inner rod.

Chapter 5

Conclusion

Two mechanical end effectors to mimic *Ensis* burrowing were designed. The end effectors were based on the design of a 0.5x scale device, and were themselves 1.0x and 2.0x the scale of *Ensis*. The end effectors were designed to couple to RoboClam, a mechanical device constructed to explore the dynamics of razor clam burrowing in fluid-soil substrates.

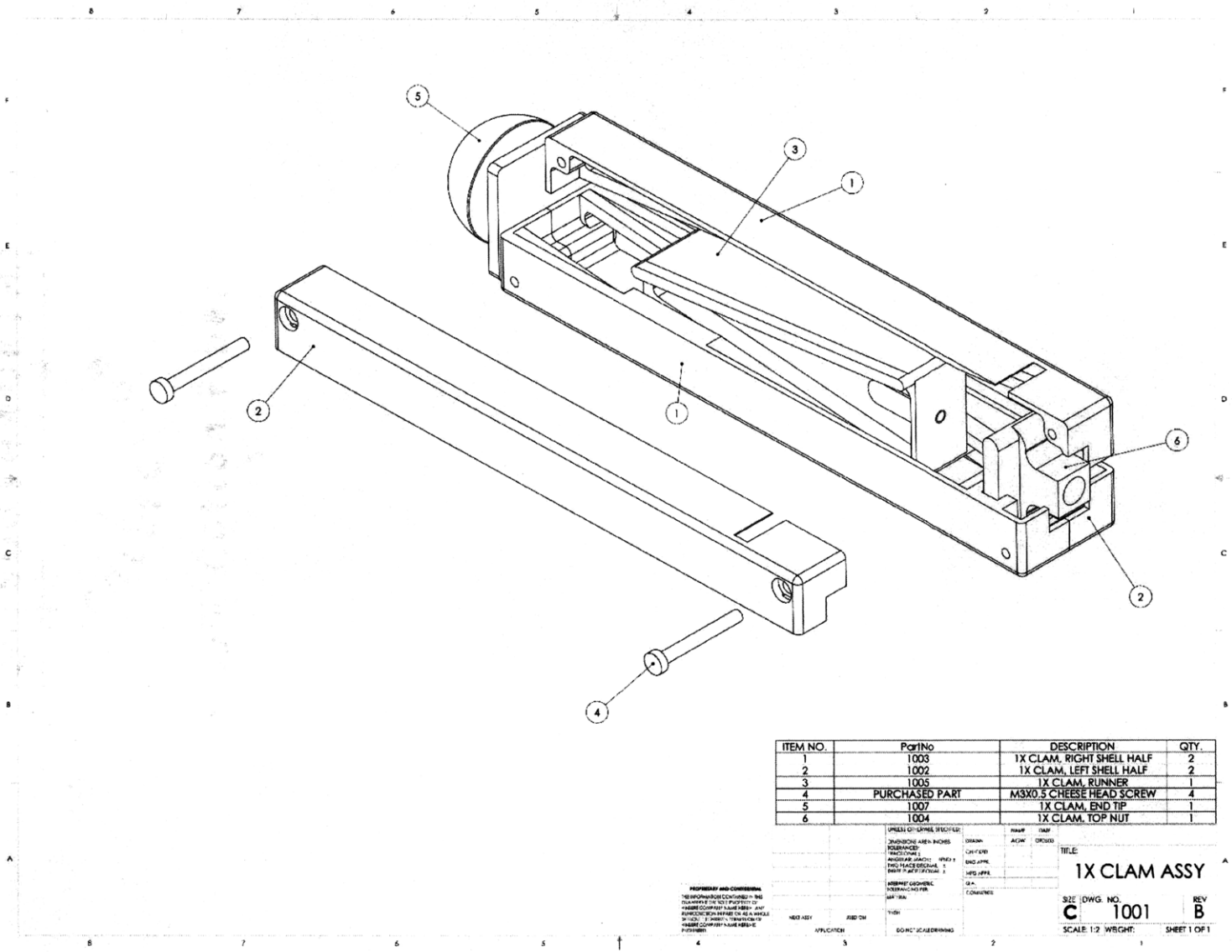
The end effectors meet the functional requirements set forth in this thesis: they are saltwater compliant, resistant to particulate, are exactly constrained and can be deterministically characterized, and can attach to the existing RoboClam apparatus.

At the time of writing, the end effectors are being manufactured. They will be tested alongside the 0.5x scale end effector when complete in order to explore the scaling relationships present in razor clam digging. The burrowing dynamics sought by this comparison can be used to make a mimetic engineering device that provides an order-of-magnitude improvement over existing technology in subsea digging and anchoring performance.

Appendix A

1.0x End Effector Drawings

This Appendix contains the engineering drawings for the 1.0x scale end effector.



ITEM NO.	PartNo	DESCRIPTION	QTY.
1	1003	1X CLAM, RIGHT SHELL HALF	2
2	1002	1X CLAM, LEFT SHELL HALF	2
3	1005	1X CLAM, RUNNER	1
4	PURCHASED PART	MSX0.5 CHEESE HEAD SCREW	4
5	1007	1X CLAM, END TIP	1
6	1004	1X CLAM, TOP NUT	1

UNLESS OTHERWISE SPECIFIED:
 DIMENSIONS ARE IN INCHES
 FINISHES: UNLESS OTHERWISE SPECIFIED
 MATERIALS: UNLESS OTHERWISE SPECIFIED
 TOLERANCES: UNLESS OTHERWISE SPECIFIED
 SURFACE FINISH: UNLESS OTHERWISE SPECIFIED
 THREADS: UNLESS OTHERWISE SPECIFIED
 HOLE TYPES: UNLESS OTHERWISE SPECIFIED
 UNLESS OTHERWISE SPECIFIED

DRAWN: []
 CHECKED: []
 ENG APPR: []
 MFG APPR: []
 QA: []
 COMMENTS: []

TITLE:
1X CLAM ASSY

SIZE: DWG NO. **C 1001** REV **B**
 SCALE: 1:2 WRIGHT SHEET 1 OF 1

Figure A-1: The 1.0x scale end effector assembly

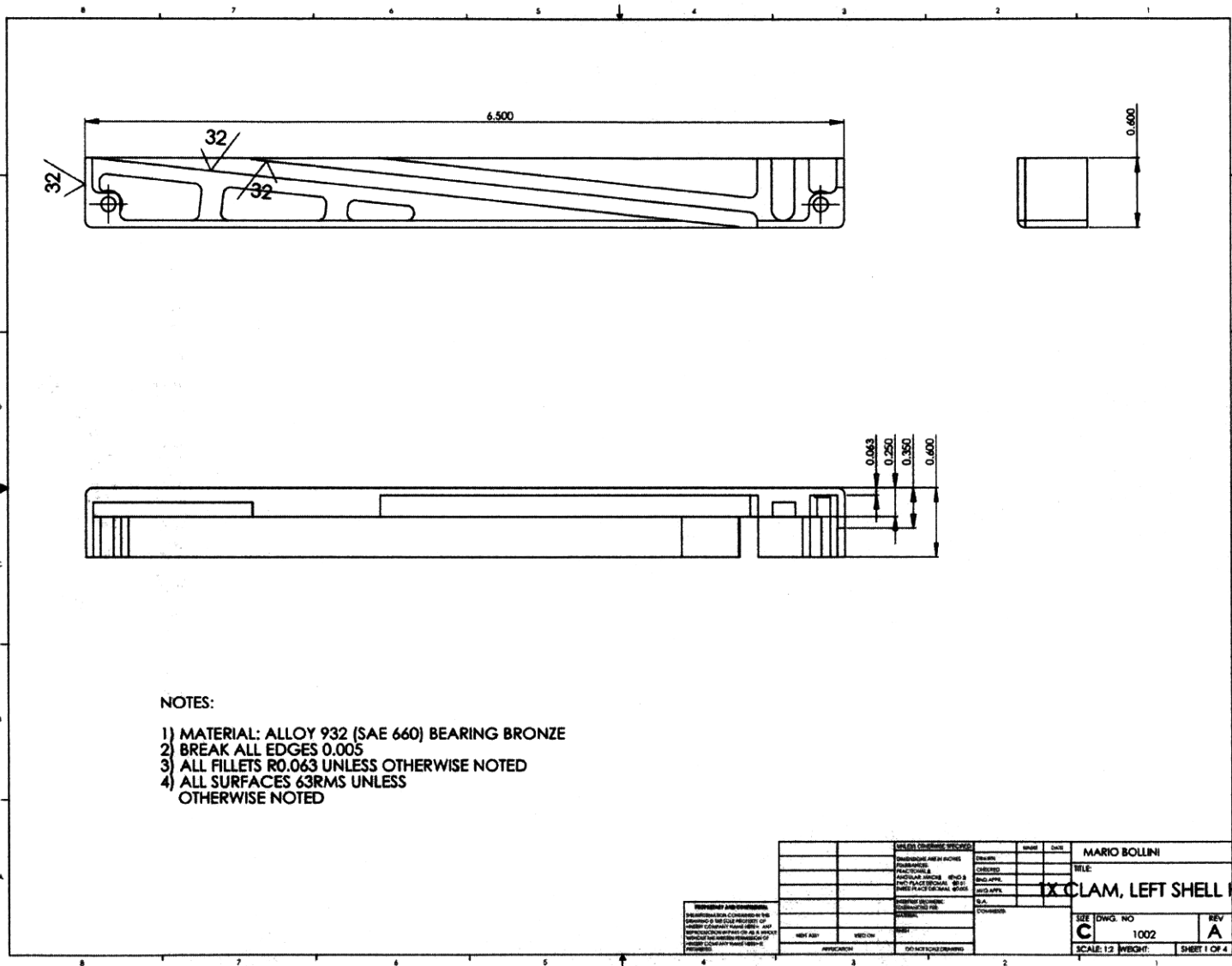


Figure A-2: The 1.0x scale left shell half (drawing 1)

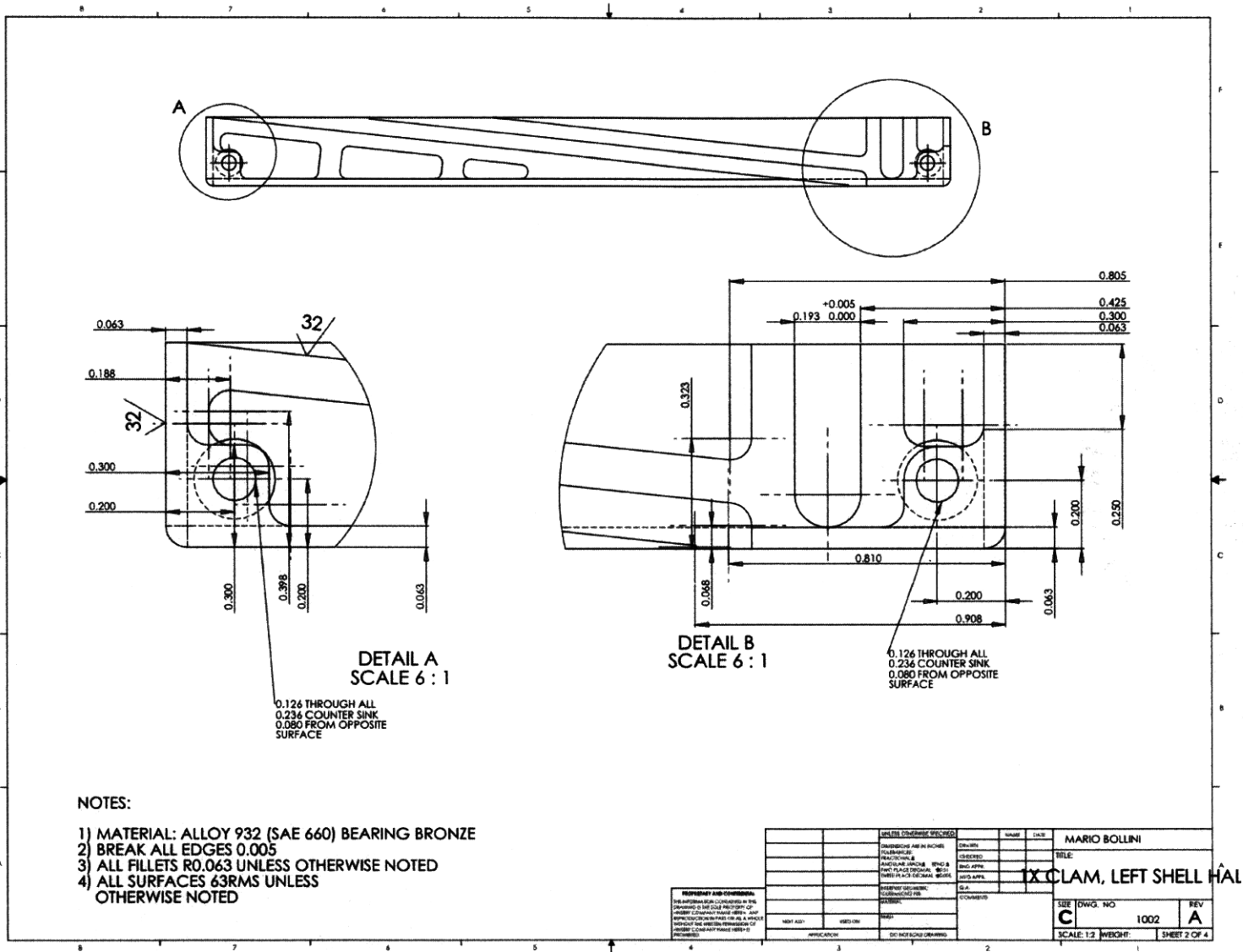


Figure A-3: The 1.0x scale left shell half (drawing 2)

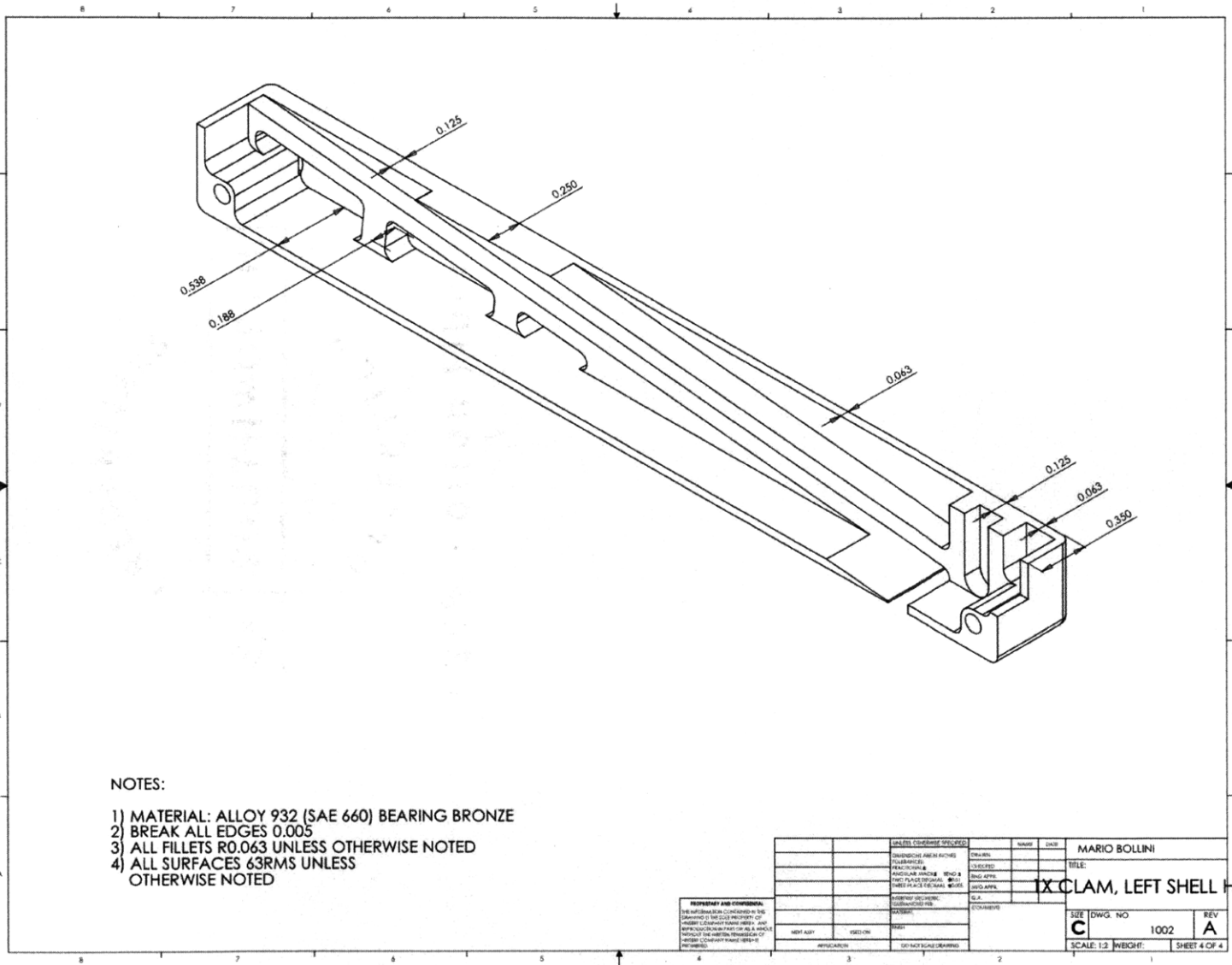


Figure A-5: The 1.0x scale left shell half (drawing 4)

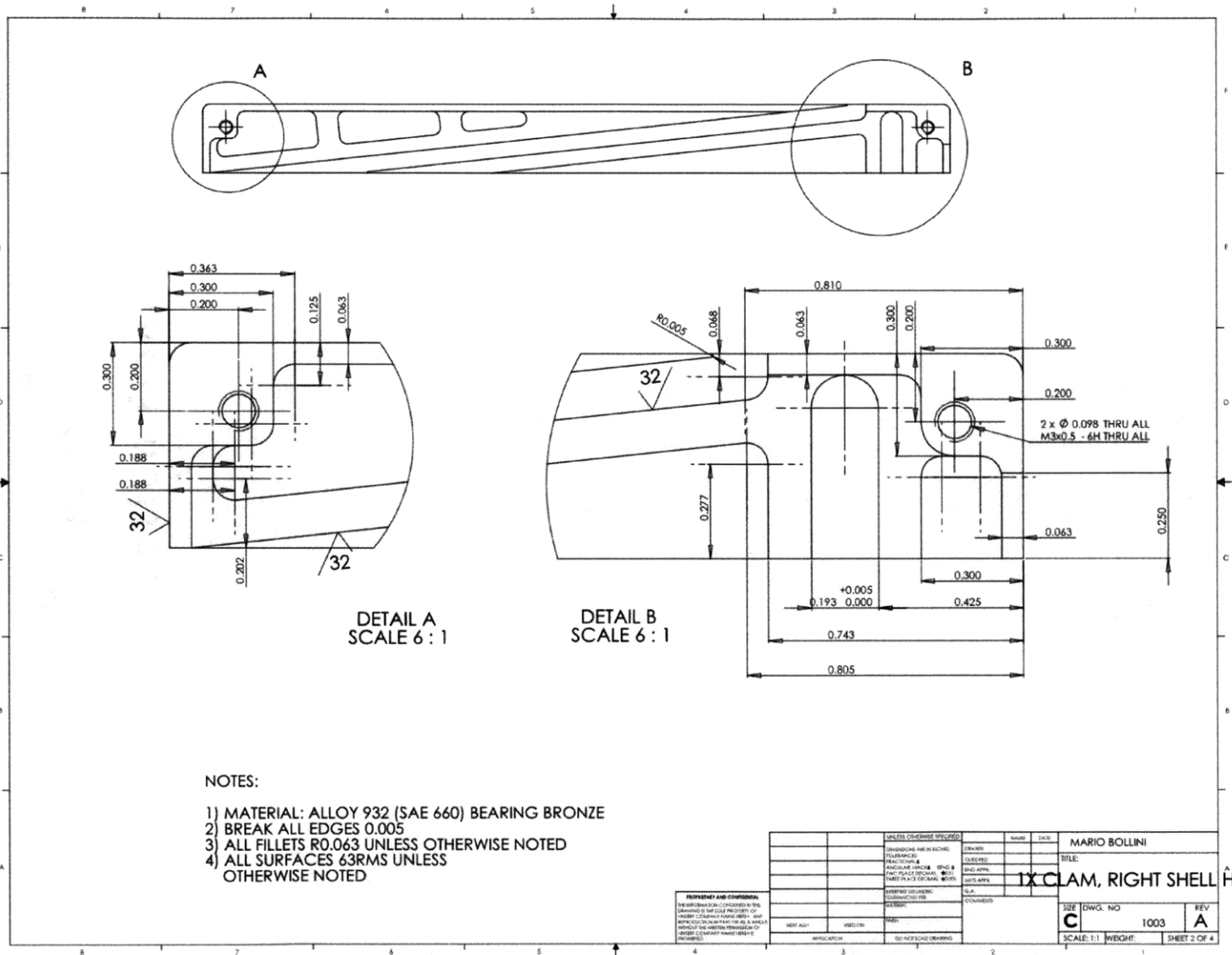


Figure A-7: The 1.0x scale right shell half (drawing 2)

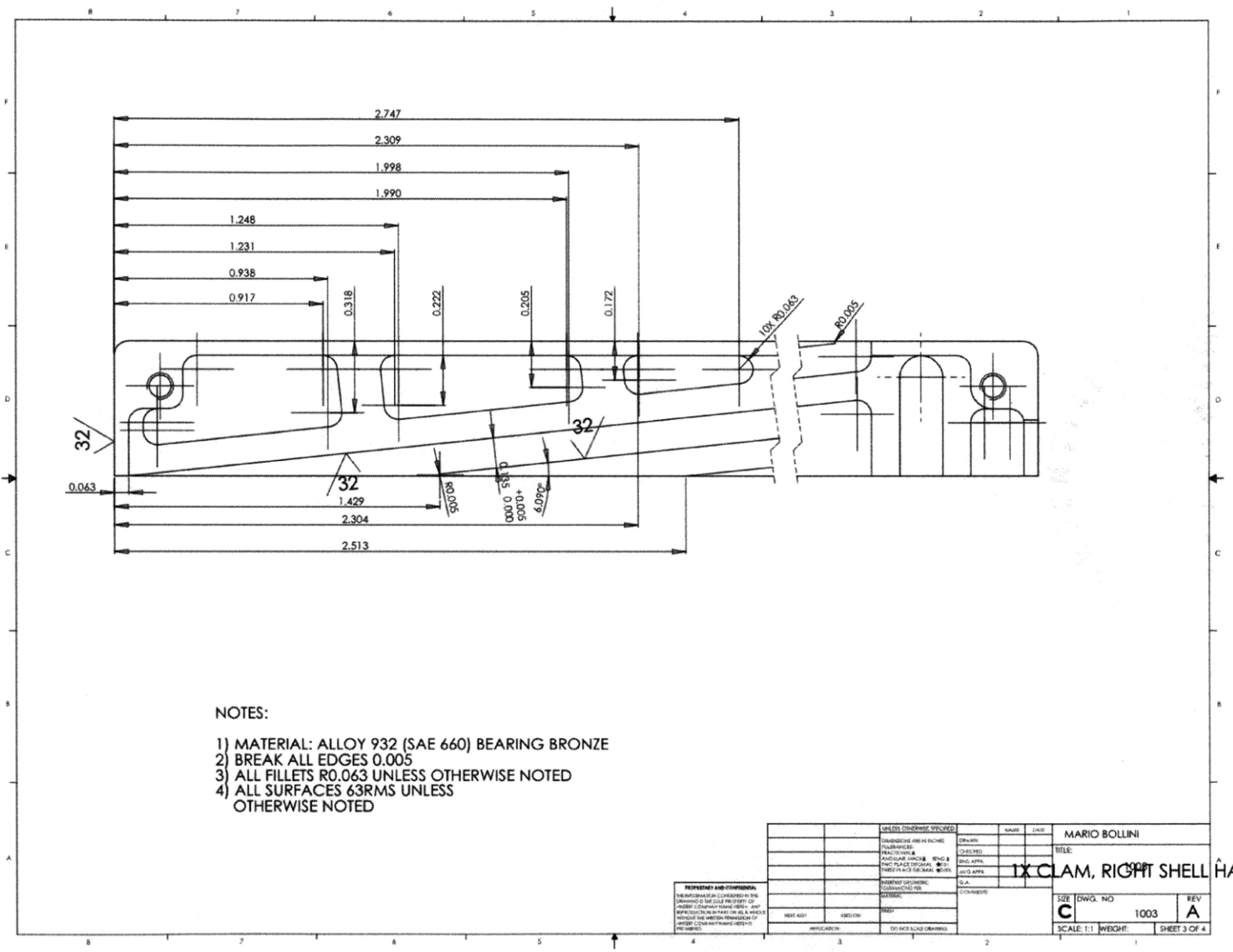


Figure A-8: The 1.0x scale right shell half (drawing 3)

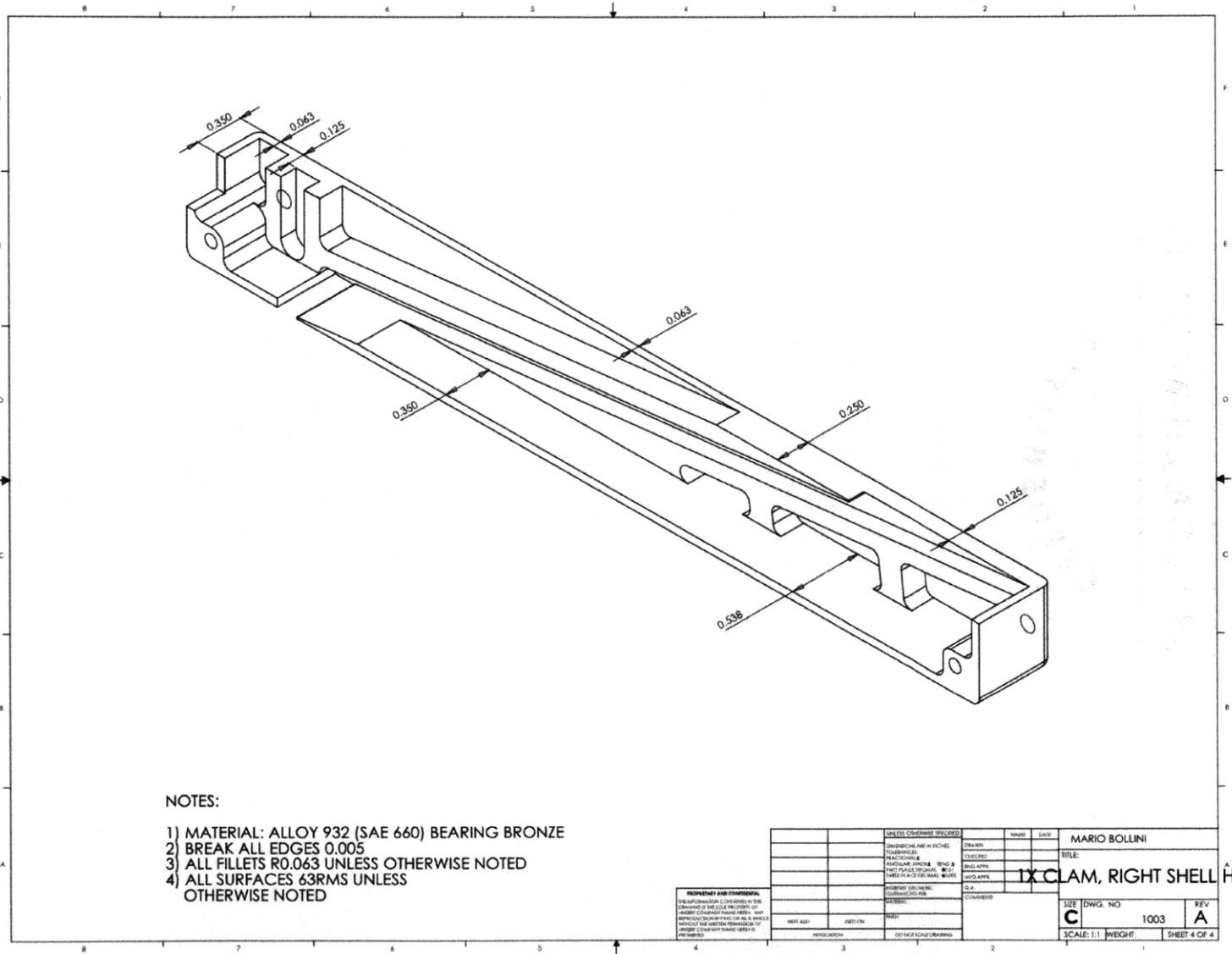


Figure A-9: The 1.0x scale right shell half (drawing 4)

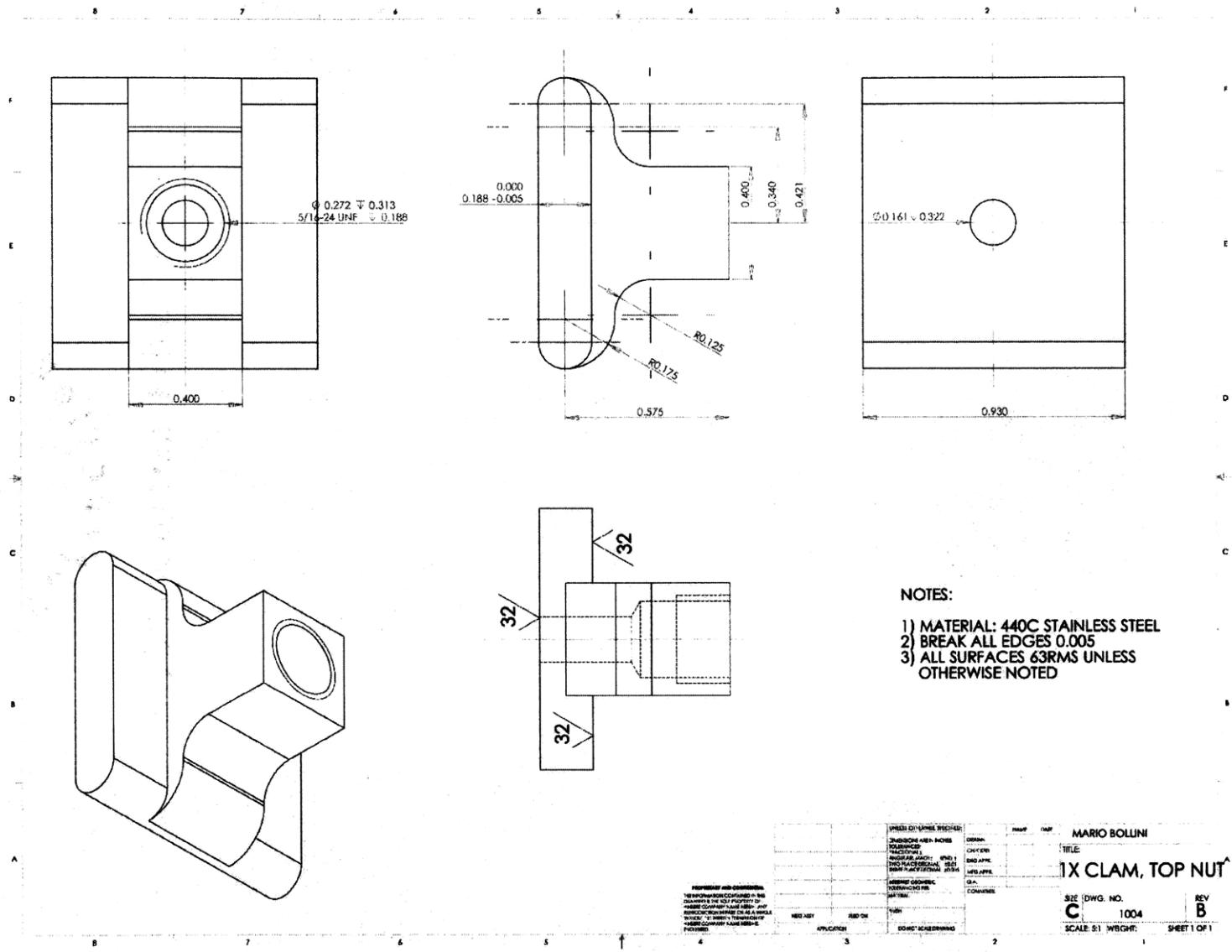
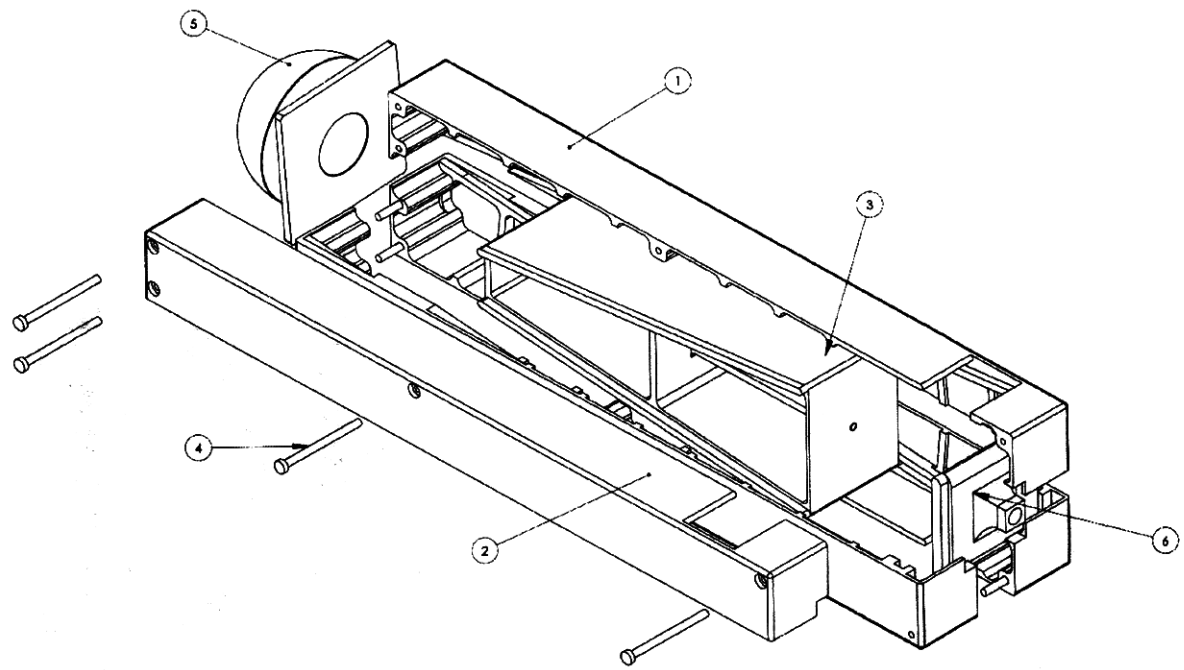


Figure A-11: The 1.0x scale top-nut

Appendix B

2.0x End Effector Drawings

This Appendix contains the engineering drawings for the 2.0x scale end effector.



ITEM NO.	PART NUMBER	DESCRIPTION	QTY.
1	2002RA-2X CLAM, LEFT SHELL HALF	2X CLAM, LEFT SHELL HALF	2
2	2003RA-2X CLAM, RIGHT SHELL HALF	2X CLAM, RIGHT SHELL HALF	2
3	2004RA-2X CLAM, WEDGE	2X CLAM, WEDGE	1
4	M3X0.5 CHEESE HEAD SCREW	M3X0.5 CHEESE HEAD SCREW	8
5	2007RA-2X CLAM, END TIP	2X CLAM, END TIP	1
6	2005RB-2X CLAM, TOP NUT		1

MARIO BOLLINI
 TITLE: 2X CLAM, ASSY
 SIZE: C DWG NO.: 2001 REV: B
 SCALE: 1:1 W8GHT: SHEET 1 OF 1

UNLESS OTHERWISE SPECIFIED:
 DIMENSIONS ARE IN INCHES
 FINISHES ARE IN INCHES
 UNLESS OTHERWISE SPECIFIED
 DIMENSIONS ARE IN MILLIMETERS
 FINISHES ARE IN MILLIMETERS
 UNLESS OTHERWISE SPECIFIED

DRAWN BY: MARIO BOLLINI
 CHECKED BY: MARIO BOLLINI
 DATE: 11/11/01

Figure B-1: The 2.0x scale end effector assembly

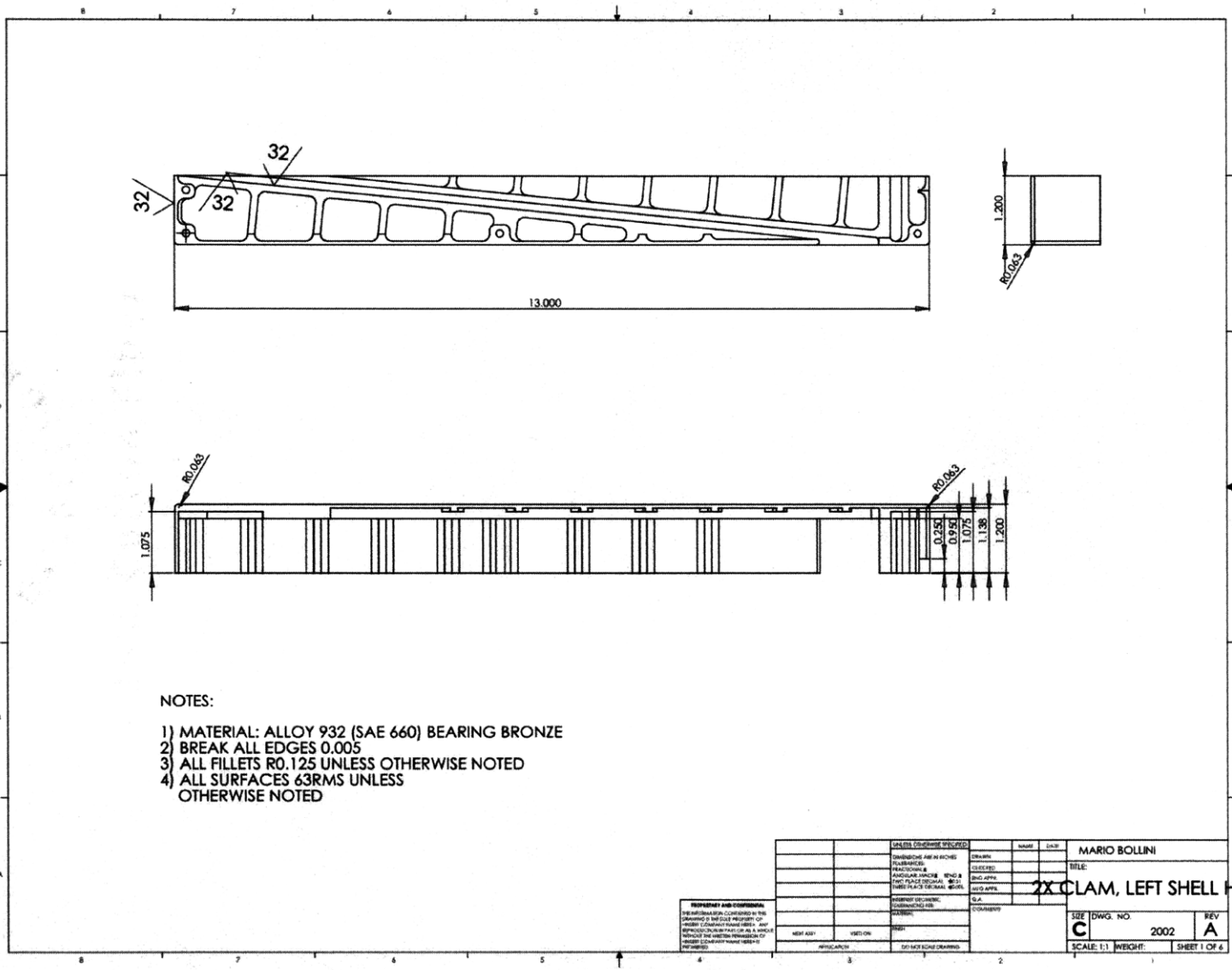


Figure B-2: The 2.0x scale left shell half (drawing 1)

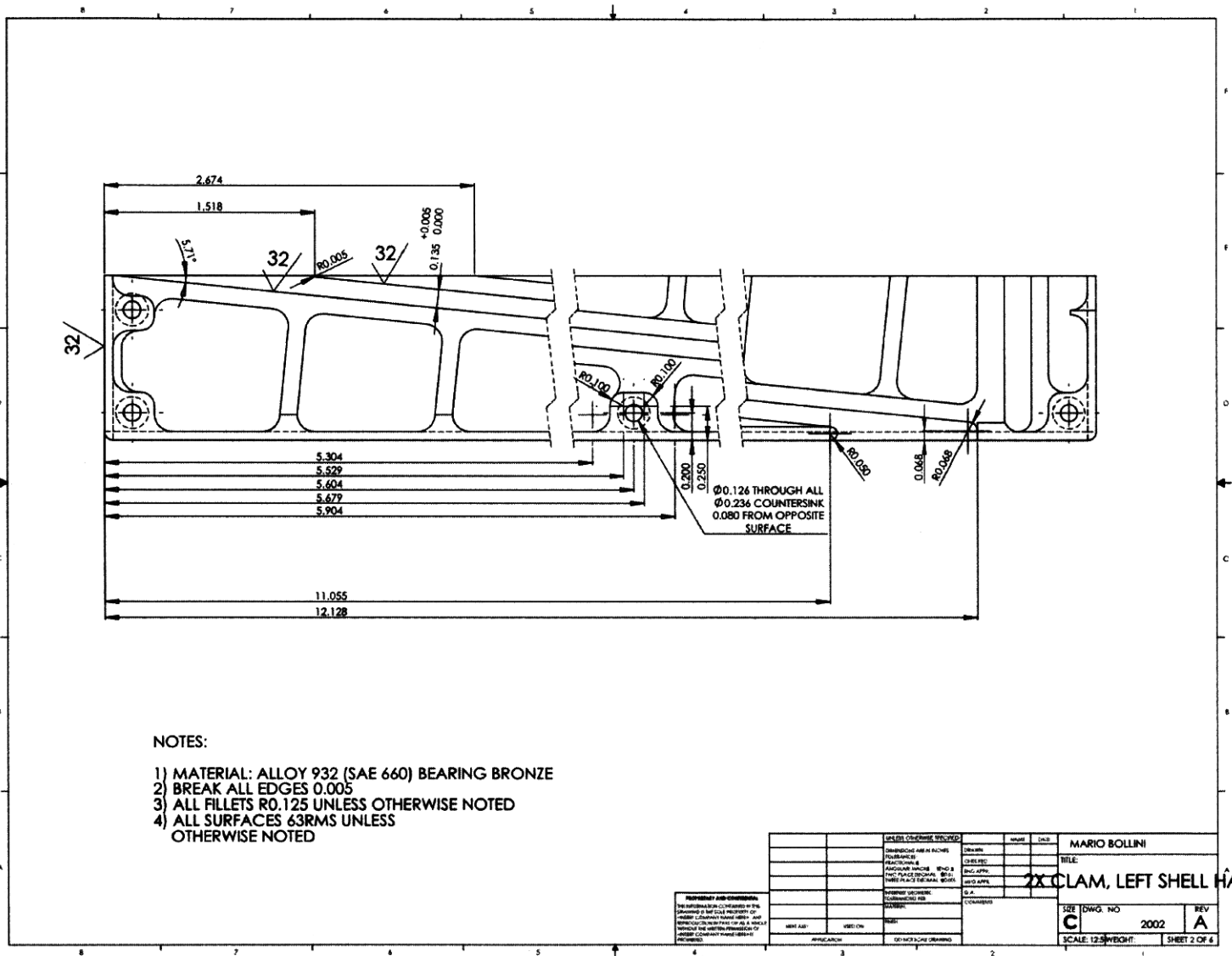


Figure B-3: The 2.0x scale left shell half (drawing 2)

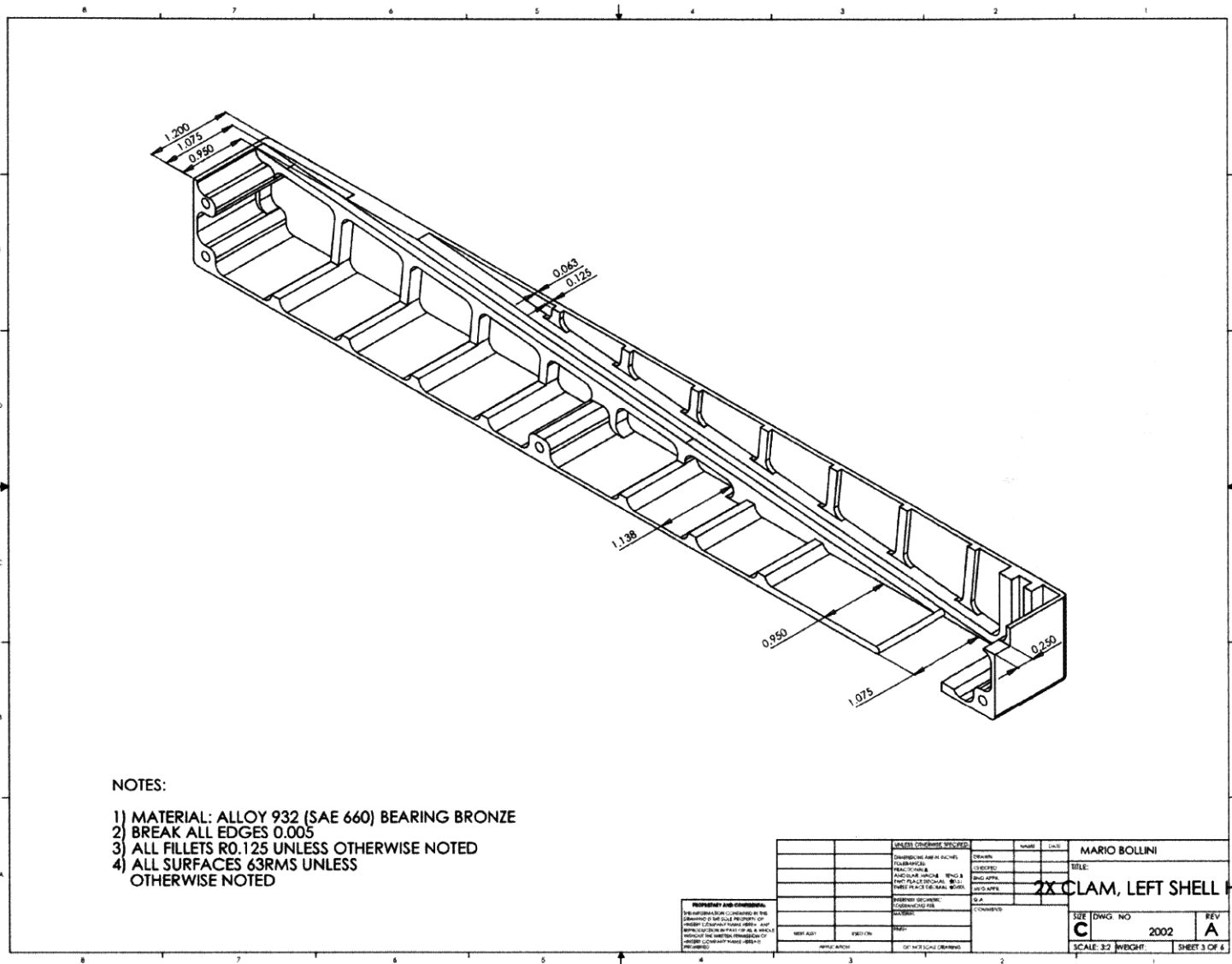


Figure B-4: The 2.0x scale left shell half (drawing 3)

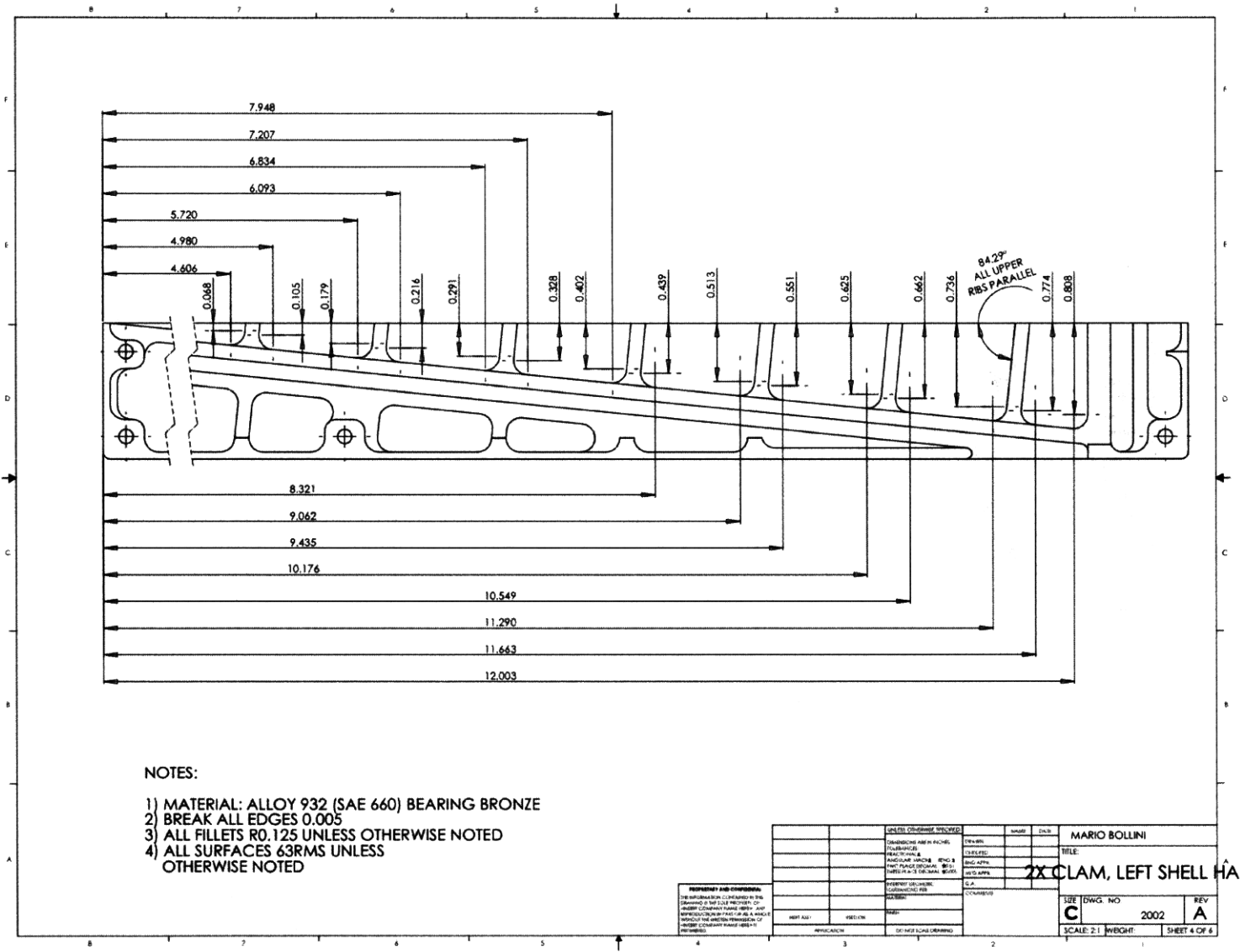


Figure B-5: The 2.0x scale left shell half (drawing 4)

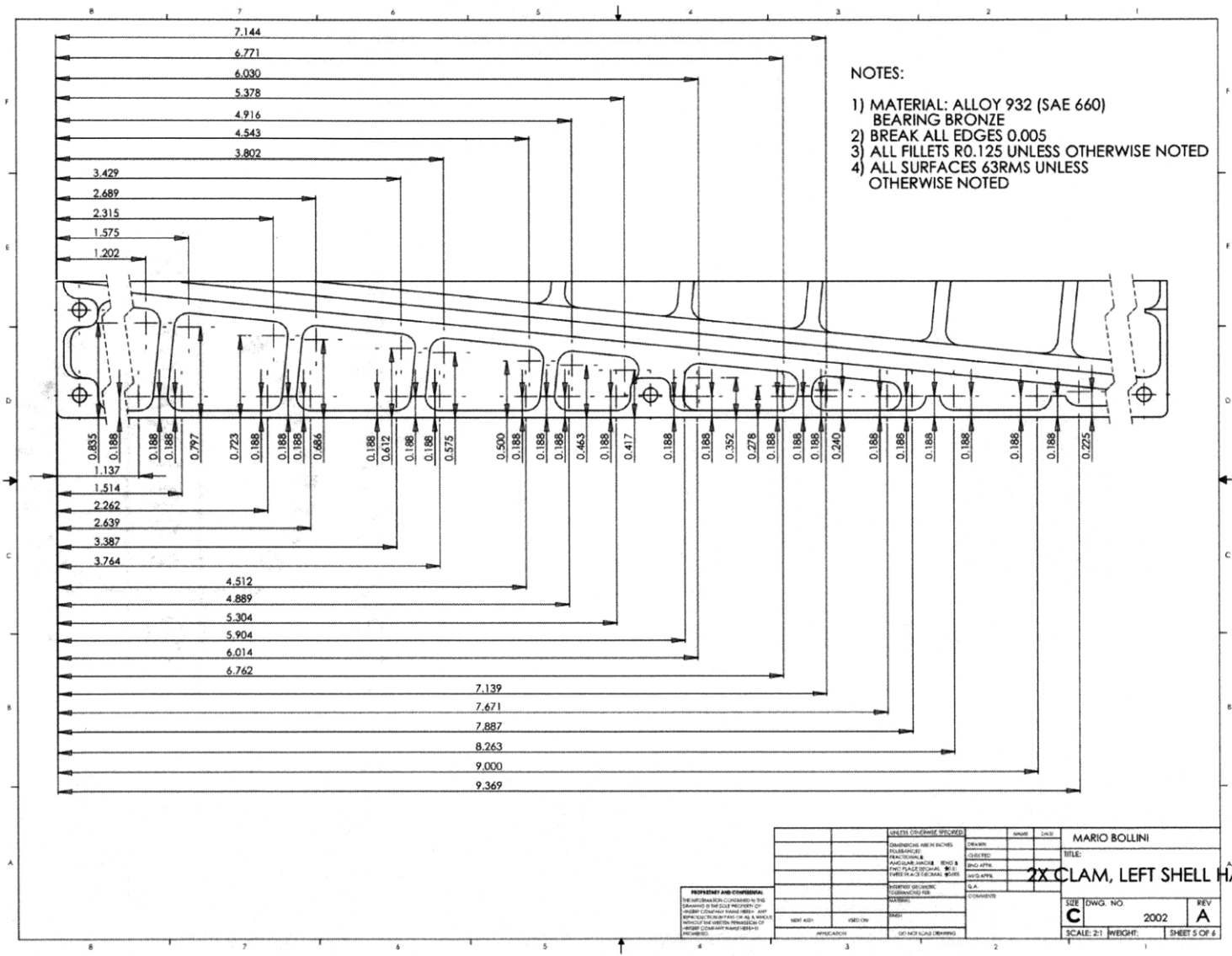


Figure B-6: The 2.0x scale left shell half (drawing 5)

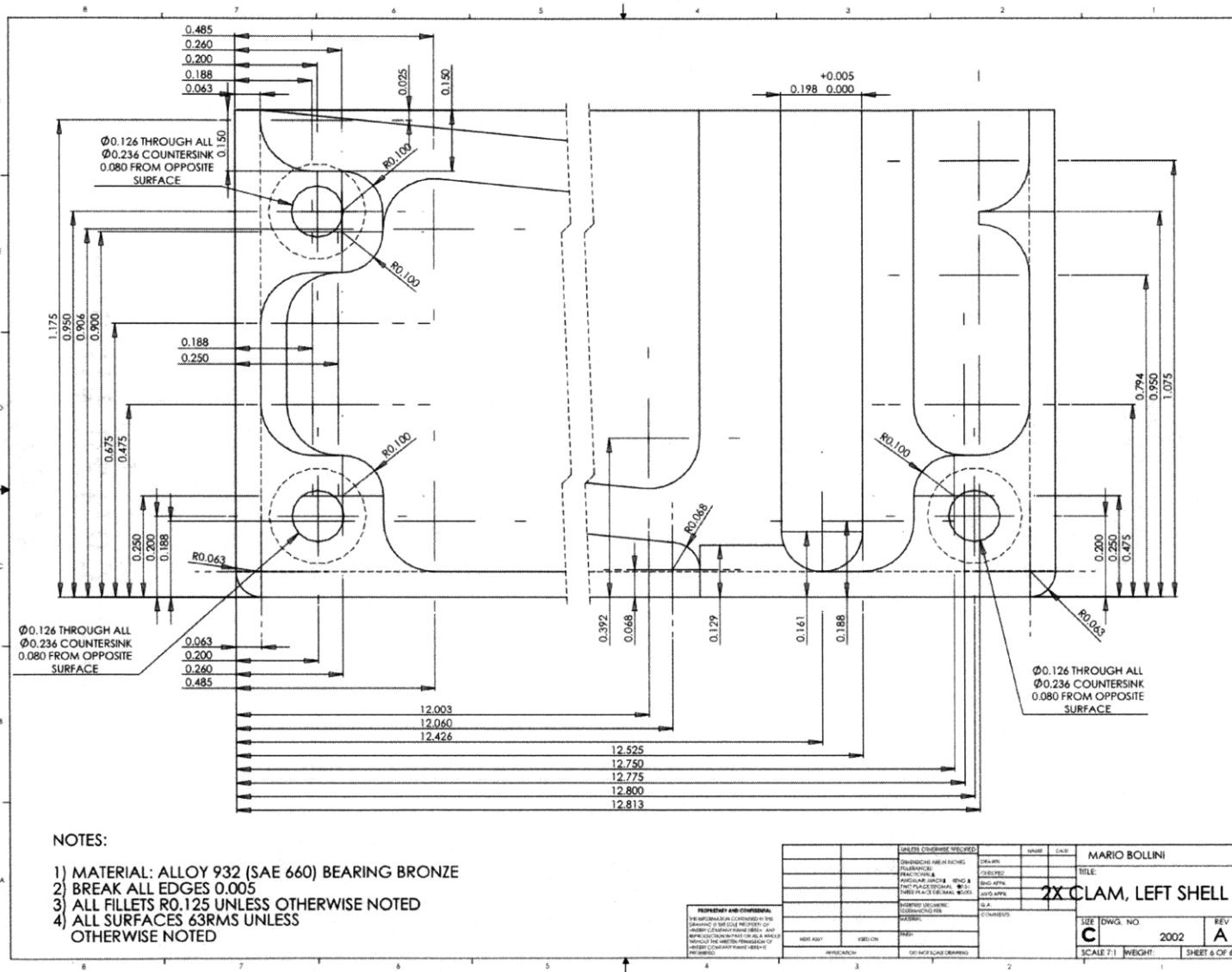


Figure B-7: The 2.0x scale left shell half (drawing 6)

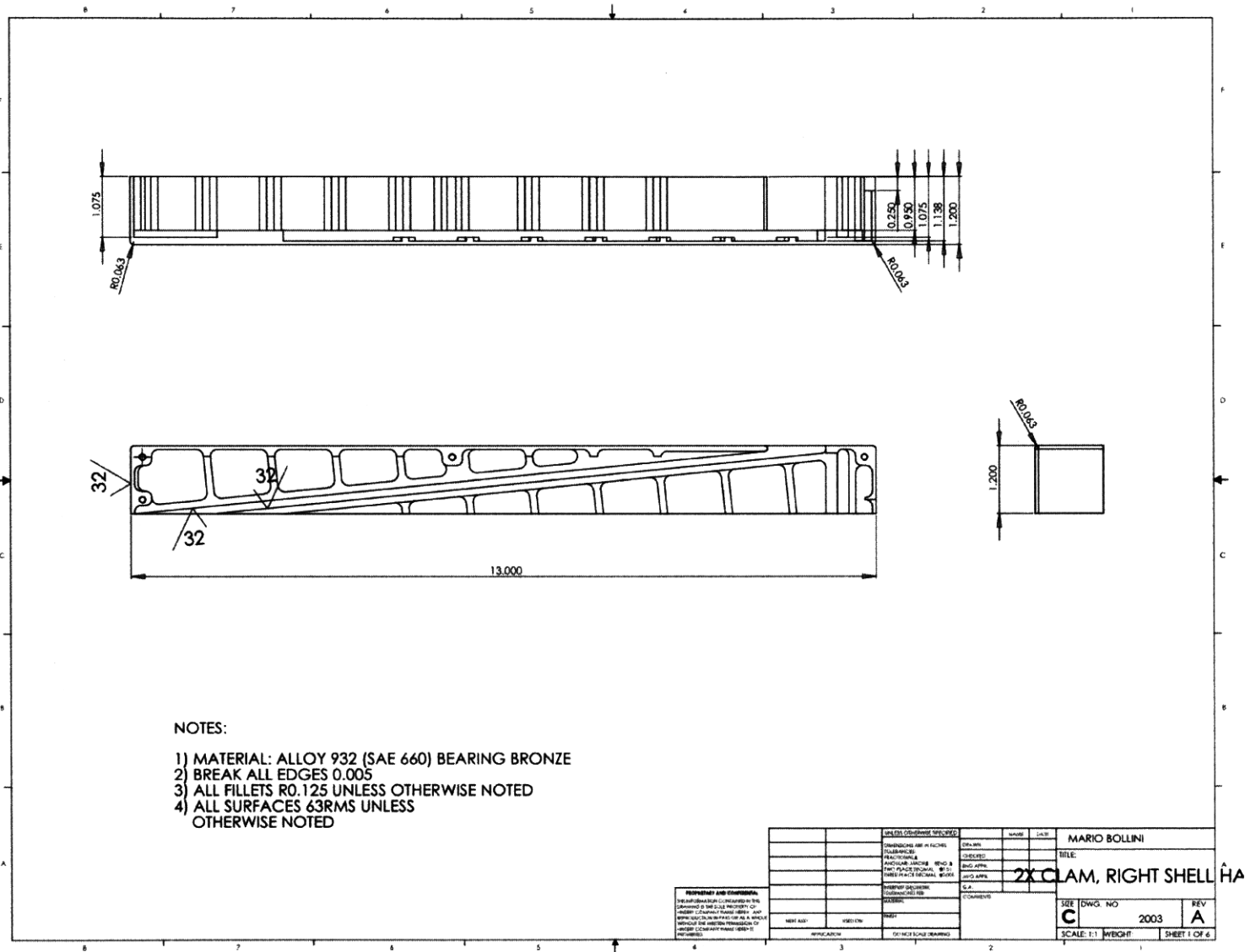


Figure B-8: The 2.0x scale right shell half (drawing 1)

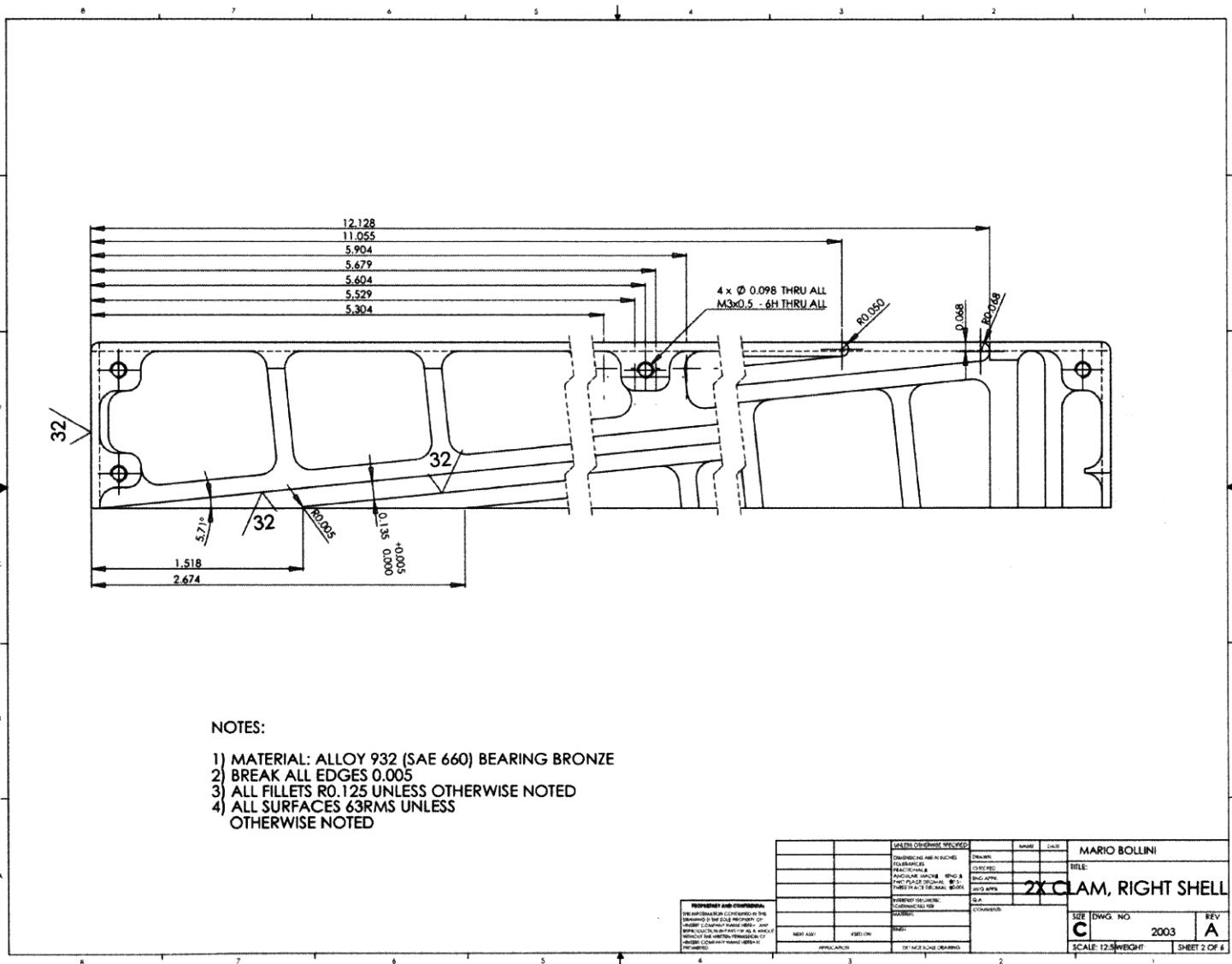


Figure B-9: The 2.0x scale right shell half (drawing 2)

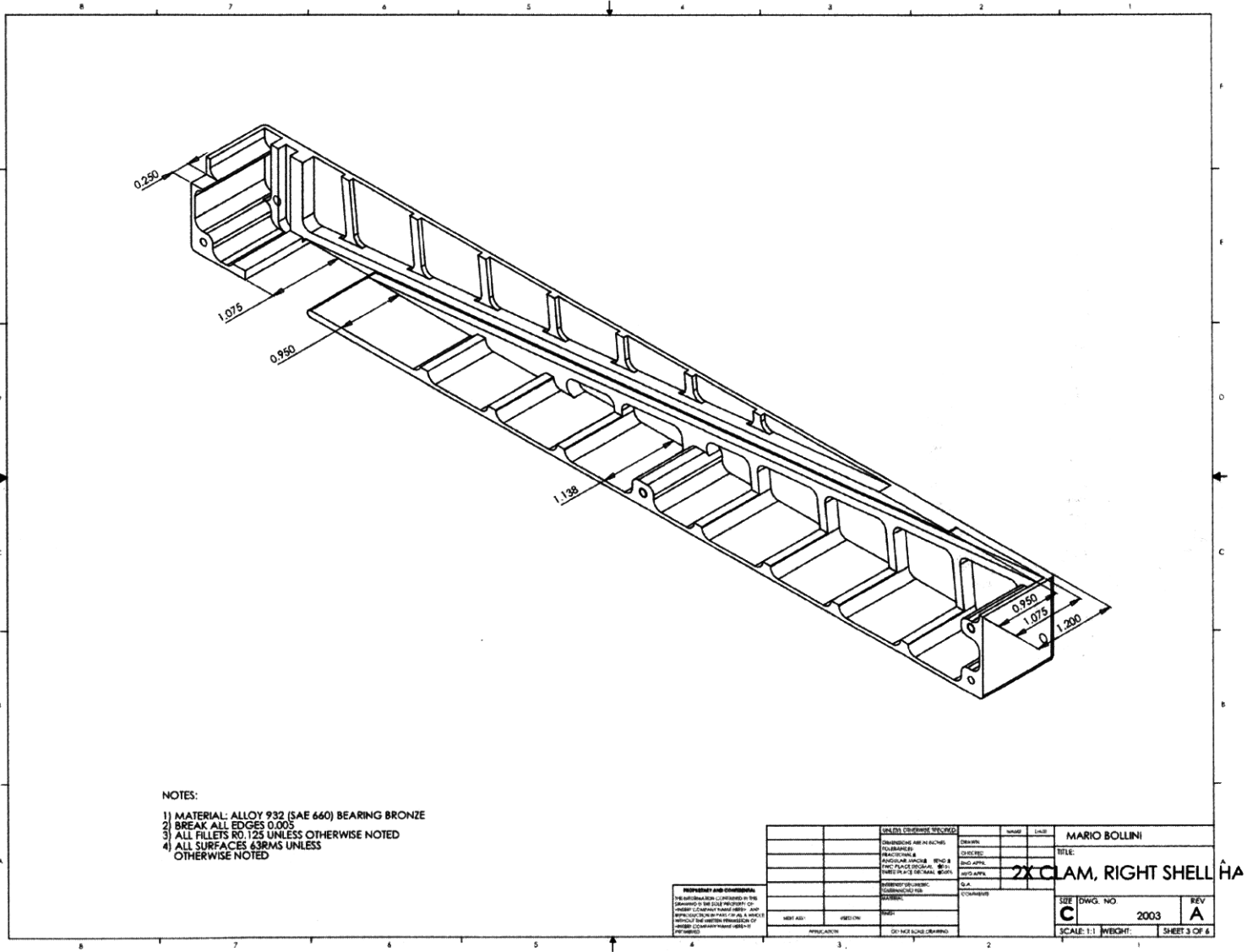


Figure B-10: The 2.0x scale right shell half (drawing 3)

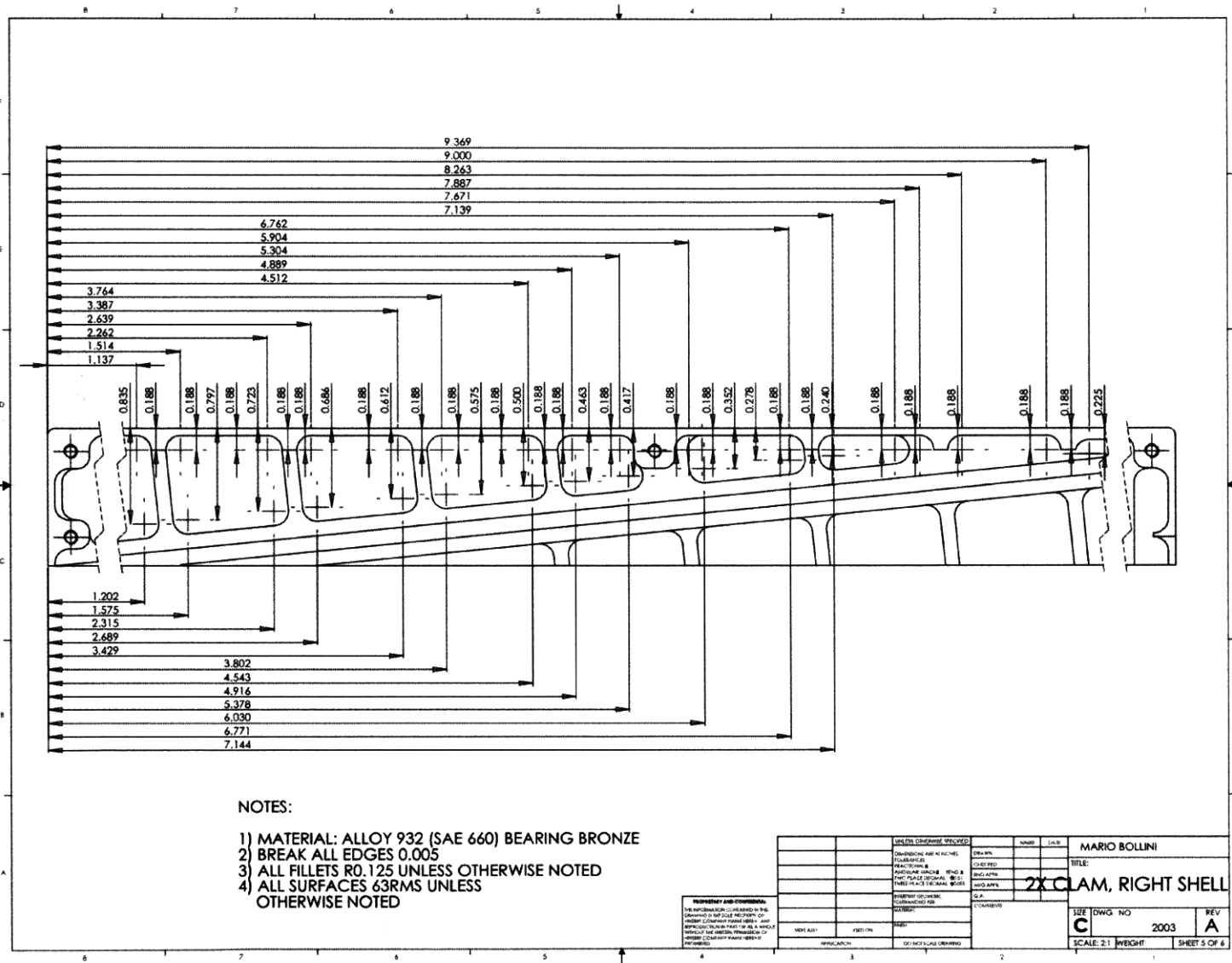


Figure B-12: The 2.0x scale right shell half (drawing 5)

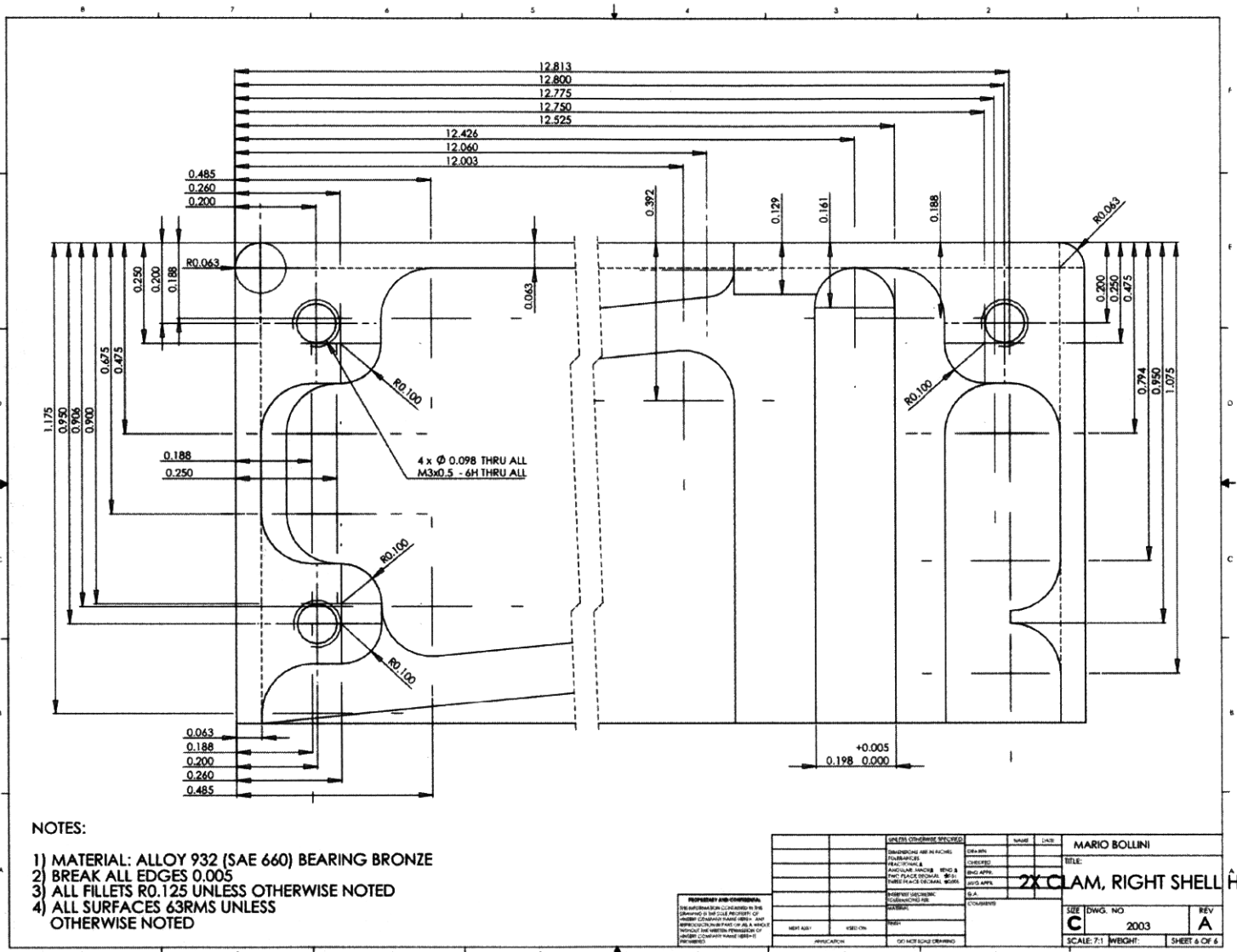
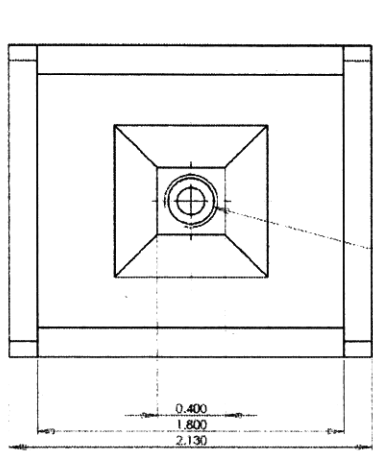
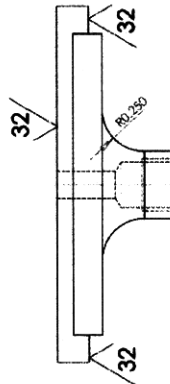
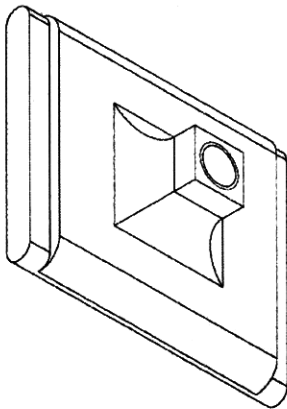
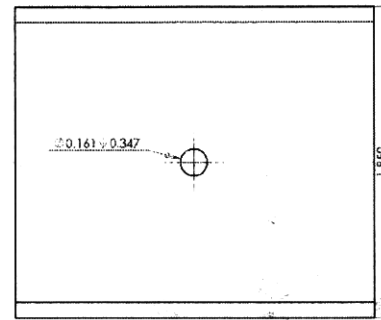
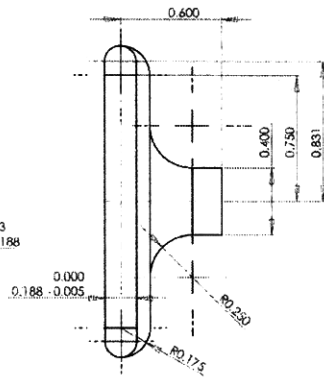


Figure B-13: The 2.0x scale right shell half (drawing 6)



$\varnothing 0.272 \pm 0.013$
 5/16-24 UNF ± 0.188



NOTES:

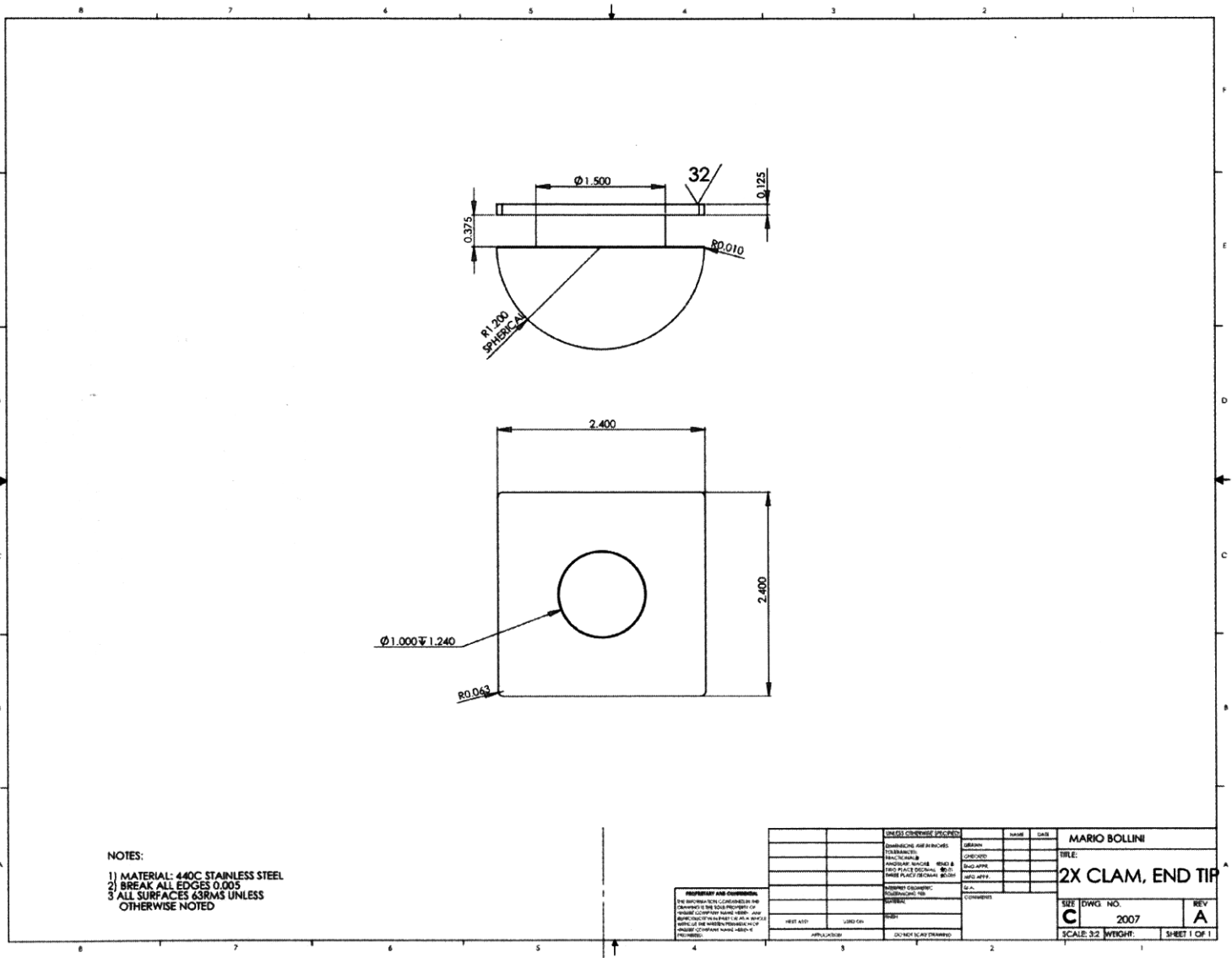
- 1) MATERIAL: 440C STAINLESS STEEL
- 2) BREAK ALL EDGES 0.005
- 3) ALL SURFACES 63RMS UNLESS OTHERWISE NOTED

PREPARED AND CHECKED BY: MARIO BOLLINI
 DRAWING NO.: 2.0X ROBOCLAM
 DATE: 10/10/2011

APPROVED	DATE
DESIGNED	DATE
CHECKED	DATE
DRAWN	DATE
SCALE	DATE

MARIO BOLLINI
 TITLE: **TOP NUT**
2.0X ROBOCLAM
 SIZE: C DWG. NO.: B
 SCALE: 5:2 WBGH: SHEET 1 OF 1

Figure B-15: The 2.0x scale top-nut



- NOTES:
- 1) MATERIAL: 440C STAINLESS STEEL
 - 2) BREAK ALL EDGES 0.005
 - 3) ALL SURFACES 63RMS UNLESS OTHERWISE NOTED

PROPRIETARY AND CONFIDENTIAL
 THE INFORMATION CONTAINED HEREIN IS THE SOLE PROPERTY OF
 ORIGINATOR AND IS TO BE KEPT IN STRICTLY CONFIDENTIAL MANNER.
 NO PART OF THIS DRAWING IS TO BE REPRODUCED OR TRANSMITTED IN ANY FORM OR BY ANY MEANS, ELECTRONIC OR MECHANICAL, INCLUDING PHOTOCOPYING, RECORDING, OR BY ANY INFORMATION STORAGE AND RETRIEVAL SYSTEM.
 ORIGINATOR: [Redacted]

UNLESS OTHERWISE SPECIFIED		NAME	DATE
DESIGNER	DATE	MARIO BOLLINI	
TRAINER	DATE		
INSPECTOR	DATE		
APPLICATOR	DATE		
TEST AUST	DATE		
USED ON			
APPLICATOR	DATE		

TITLE:	
2X CLAM, END TIP	
SIZE	DWG. NO.
C	2007
SCALE: 3:2	WEIGHT:
	SHEET 1 OF 1

Figure B-16: The 2.0x scale end tip

Bibliography

- [1] Amos G. Winter, V et. al. The design and testing of roboclam: A machine used to investigate and optimize razor clam-inspired burrowing mechanisms for engineering applications. Accepted for inclusion in International Design Engineering Technical Conferences & Computers and Information in Engineering Conference. ASME, 2009.
- [2] E.R. Trueman, A.R. Brand, and P. Davis. The dynamics of burrowing of some common littoral bivalves. *Journal of Experimental Biology*, 44(3):469–492, 1966.
- [3] E.R. Trueman. Bivalve mollusks: Fluid dynamics of burrowing. *Science*, 152(3721):523–525, 1966.
- [4] A.F. Holland and J.M. Dean. Biology of stout razor clam tagelus-plebius .1. animal-sediment relationships, feeding mechanism, and community biology. *Chesapeake Science*, 18(1):58–66, 1977.
- [5] E.R. Trueman. The dynamics of burrowing in ensis (bivalvia). volume 166 of *B, Biological Sciences*, pages 459–476, 1967.
- [6] Stainless steel 304. <http://www.lenntech.com/Stainless-steel-304.htm>.
- [7] Joseph E. Shigley and Charles R. Mischke. *Mechanical Engineering Design (in SI Units)*. Tata McGraw Hill, New Delhi, 6 edition, 2001.
- [8] E.A. Avallone and I.T. Baumeister. *Mark's Standard Handbook for Mechanical Engineers*. McGraw-Hill, New York, 10 edition, 1996.
- [9] MatWeb. High-leaded tin bronze, uns c93200, copper casting alloy, bearing bronze 660. <http://www.matweb.com/search/DataSheet.aspx?MatGUID=b673f55f412f40ae9ee03e9986747016>.
- [10] BearTech Alloys. Nickel aluminum bronze. <http://www.beartechalloys.com/typec958.html>.
- [11] Properties of stainless steel aisi type 440c. <http://www.efunda.com/Materials/alloys>.
- [12] MatWeb. Kinetics mim 440c stainless steel. <http://www.matweb.com/search/DataSheet.aspx?MatGUID=f4e8f63ce59c4168a41ce6084dcdd9a96ckck=1>.